Transactions of Tianjin University (2022) 28:245–264
https://doi.org/10.1007/s12209-022-00326-x

REVIEW

# Heterogeneous Catalysis for $CO_2$ Conversion into Chemicals and Fuels

**Dunfeng Gao[1] · Wanjun Li[1] · Hanyu Wang[1,2] · Guoxiong Wang[1] · Rui Cai[1]**

Received: 20 May 2022 / Revised: 7 June 2022 / Accepted: 9 June 2022 / Published online: 9 August 2022


## Abstract

Catalytic conversion of $CO_2$ into chemicals and fuels is a viable method to reduce carbon emissions and achieve carbon neutrality. Through thermal catalysis, electrocatalysis, and photo(electro)catalysis, $CO_2$ can be converted into a wide range of valuable products, including CO, formic acid, methanol, methane, ethanol, acetic acid, propanol, light olefins, aromatics, and gasoline, as well as fine chemicals. In this mini-review, we summarize the recent progress in heterogeneous catalysis for $CO_2$ conversion into chemicals and fuels and highlight some representative studies of different conversion routes. The structure–performance correlations of typical catalytic materials used for the $CO_2$ conversion reactions have been revealed by combining advanced in situ/operando spectroscopy and microscopy characterizations and density functional theory calculations. Catalytic selectivity toward a single $CO_2$ reduction product/fraction should be further improved at an industrially relevant $CO_2$ conversion rate with considerable stability in the future.

## Graphical Abstract

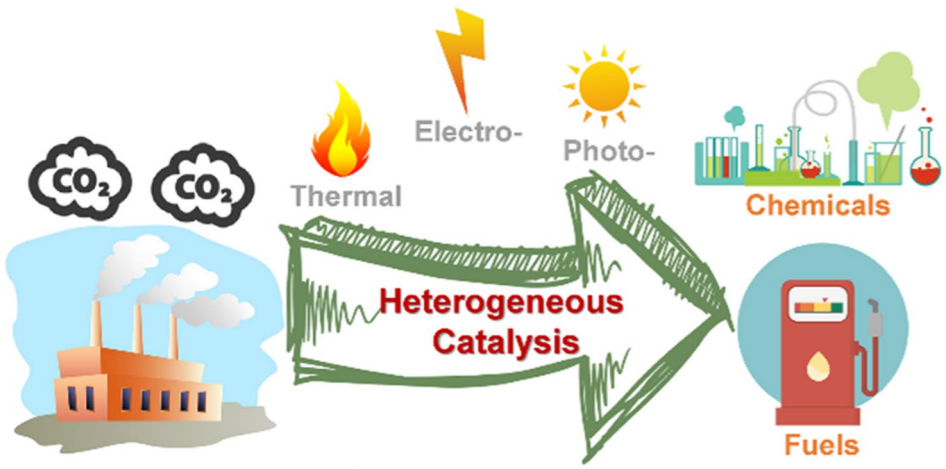


**Keywords** $CO_2$ conversion · $CO_2$ hydrogenation · $CO_2$ electroreduction · Chemicals · Fuels

✉ Guoxiong Wang
wanggx@dicp.ac.cn

✉ Rui Cai
cairui@dicp.ac.cn

[1] State Key Laboratory of Catalysis, Dalian National Laboratory for Clean Energy, Dalian Institute of Chemical Physics, Chinese Academy of Sciences, Dalian 116023, China

[2] University of Chinese Academy of Sciences, Beijing 100049, China

## Introduction

Since the industrial revolution, the $CO_2$ concentration in the atmosphere has been rapidly increasing because of fossil fuel utilization and human activities, resulting in severe climate change due to the significant greenhouse effect of $CO_2$. To address this issue, global carbon emissions need to be reduced, and China has set its goal of achieving carbon neutrality by 2060. Carbon capture, utilization, and storage

(CCUS) is an important emission reduction technology that can effectively utilize highly concentrated $CO_2$ emitted by industrial activities. Among the CCUS processes, $CO_2$ utilization via catalytic conversion is promising as it provides a viable solution to close the carbon cycle [1–6].

Generally, the $CO_2$ molecule is thermodynamically stable and kinetically inert; thus, $CO_2$ activation is an important scientific challenge. $CO_2$-conversion-related chemical reactions require remarkable energy input in the chemical, thermal, or electrical form. If the energy comes from fossil fuels, then the process would not achieve the net reduction of $CO_2$. Therefore, $CO_2$ conversion should be driven by nonfossil energy sources, such as nuclear energy and renewable energy, such as solar and wind. Catalysis is an efficient method to activate and convert inert molecules and plays a crucial role in $CO_2$ conversion into valuable chemicals and fuels (e.g., CO, formic acid, methanol, methane, ethanol, acetic acid, propanol, light olefins, aromatics, and gasoline). The substantial amount of hydrogen needed in the production of chemicals and fuels from catalytic $CO_2$ conversion (mainly $CO_2$ reduction) should come from water indirectly in thermal catalysis or directly in electrocatalysis and photo(electro)catalysis [2].

To date, many research institutions in the world have devoted tremendous efforts to the field of catalytic $CO_2$ conversion. As one of the leading research institutions for fundamental and applied catalysis in the world, the Dalian Institute of Chemical Physics (DICP) started its research on heterogeneous catalysis for $CO_2$ conversion in the early 1990s in the field of thermal catalysis [7] and has expanded the research to electrocatalytic and photo(electro)catalytic $CO_2$ conversion in the past decade [8, 9] (Fig. 1). Some important concepts (e.g., nanoconfined catalysis and single-atom catalysis) in heterogeneous catalysis proposed by our institute have also been applied to catalytic $CO_2$ conversion [10, 11]. In this review, we summarize our recent progress in heterogeneous catalysis for $CO_2$ conversion into chemicals and fuels in different conversion routes and highlight some representative studies of thermal catalysis, electrocatalysis, and photo(electro)catalysis.

## Thermocatalytic $CO_2$ Conversion

$CO_2$ conversion via thermal catalysis involves a large group of catalytic reactions, including $CO_2$ hydrogenation, dry reforming of methane with $CO_2$, and nonreductive $CO_2$ conversion into fine chemicals. Of these routes, direct $CO_2$ hydrogenation to valuable chemicals and fuels is most promising. As more than 90% of industrial hydrogen is currently

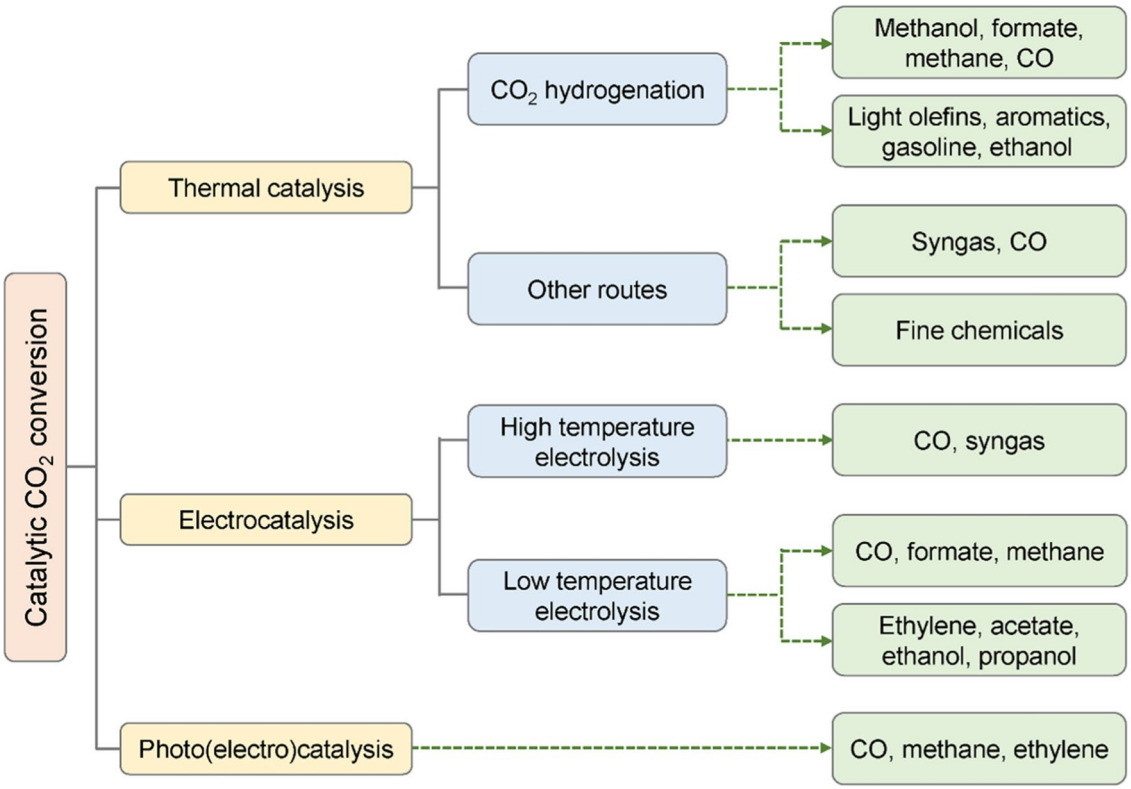


**Fig. 1** Heterogeneous catalysis routes for $CO_2$ conversion into chemicals and fuels

produced from fossil fuels via steam reforming of natural gas and coal gasification, which in turn produce substantial $CO_2$, $CO_2$ hydrogenation should proceed using hydrogen produced in a manner free of $CO_2$ emission. Obtaining hydrogen via water electrolysis powered by renewable energy sources provides a viable solution to this issue, thus making $CO_2$ hydrogenation attractive.

## $CO_2$ Hydrogenation to $C_1$ Products

Methanol, formic acid, methane, and CO are the four main $C_1$ products synthesized from $CO_2$ hydrogenation. In light of the reaction thermodynamics (Table 1), $CO_2$ hydrogenation to most $C_1$ products is exothermic, except for CO production via an endothermic reverse water gas shift (RWGS) reaction. Although the $\Delta G^0_{298\,K}$ value of $CO_2$ hydrogenation to formic acid is positive, in most studies adding a base to the reaction medium shifts the reaction equilibrium forward, thereby making the reaction easier and yielding formate as the final product. The generation of methanol, methane, and CO from $CO_2$ hydrogenation is often concurrent under their required reaction conditions, thereby developing efficient catalysts with high selectivity toward the desired $C_1$ products and considerably improving activity and stability.

### Methanol

Methanol synthesis from $CO_2$ and hydrogen is the first target based on the concept of "liquid sunshine" proposed by Bai and coworkers [12]. Methanol can be used as either liquid fuel or platform molecule for subsequent upgrading to higher-value chemicals via emerging technologies, such as the methanol to olefins process [13]. $CO_2$ hydrogenation to methanol occurs at 200 °C to 300 °C and 3–10 MPa, under which conditions the RWGS and $CO_2$ methanation reactions are also thermodynamically favorable. $Cu/ZnO/Al_2O_3$ is an industrial catalyst for traditional methanol synthesis from syngas ($CO + H_2$). This catalyst is also applied to methanol synthesis from $CO_2$ hydrogenation. However, $Cu/ZnO/Al_2O_3$ is also an active catalyst for the RWGS reaction, resulting in a low methanol selectivity. Moreover, $CO_2$ hydrogenation produces more water, which causes severe sintering and deactivation of Cu catalysts [14]. The methanol selectivity is usually lower than 50% at a considerable $CO_2$ conversion (i.e., > 10%) over traditional $Cu/ZnO/Al_2O_3$ catalysts [15].

The reactivity and stability of Cu-based catalysts can be improved by stabilizing active Cu species via metal–support interaction enhancement. Cu catalysts supported by alternative oxides (e.g., $SiO_2$, $ZrO_2$, $CeO_2$, and $Ce_{1-x}Zr_xO_2$) have been developed [16–19]. Sun and coworkers [16] developed a $Cu^+$-enriched $Cu/SiO_2$ catalyst using the flame spray pyrolysis (FSP) method. This catalyst achieved a methanol selectivity of 79% at a $CO_2$ conversion rate of 5.2%. A unique shattuckite-like structure with slightly distorted Cu–O–Si texture in the FSP-prepared catalyst was considered to enrich the $Cu^+$ species. High-pressure in situ diffuse reflectance infrared Fourier transform spectroscopy (DRIFTS) showed that the $Cu^+$ species could stabilize and facilitate the hydrogenation of the *CO intermediate to methanol via an RWGS + CO hydrogenation pathway.

Apart from Cu-based catalysts, researchers also considered non-Cu catalytic materials, such as Pd nanoparticles (NPs) confined in carbon nanotubes, $Pd/ZnO/Al_2O_3$, $Pt/In_2O_3$, $MoS_2$, $ZnO–ZrO_2$ solid solution, and $TiO_2$-supported Cd cluster [15, 20–26]. Li and coworkers [22] reported a $ZnO–ZrO_2$ solid solution catalyst, which achieved a methanol selectivity of 86% to 91% and excellent stability for 500 h at a $CO_2$ conversion of more than 10% under the investigated reaction conditions (Fig. 2a, b). The in situ spectroscopy and theoretical calculation results indicated that the synergetic effect between Zn and Zr sites in the $ZnO–ZrO_2$ solid solution catalyst contributed to the outstanding methanol synthesis performance. A $MoS_2$ nanosheet catalyst with rich sulfur vacancies developed by Deng and coworkers [25] was able to achieve $CO_2$ hydrogenation to methanol at a low reaction temperature (180 °C) but with a methanol selectivity of 94.3% at a $CO_2$ conversion rate of 12.5% and a stable performance during a long-term test for over 3 000 h.

### Formic Acid (Formate)

Formic acid usually presents as formate in practical production from $CO_2$ hydrogenation, as thermodynamics can efficiently shift the reaction equilibrium in the forward direction ($CO_2 + H_2 \rightarrow HCOOH$; $HCOOH + OH^- \rightarrow HCOO^- + H_2O$). $CO_2$ hydrogenation to formate is generally achieved via bicarbonate hydrogenation in alkaline environments, but it suffers from high activation energy because of the considerable thermodynamic stability of the bicarbonate intermediate. Huang and coworkers [27]

**Table 1** Reaction thermodynamics of $CO_2$ hydrogenation to $C_1$ products

| Reaction | $\Delta H^0_{298K}$ (kJ/mol) | $\Delta G^0_{298K}$ (kJ/mol) |
|---|---|---|
| $CO_2\,(g) + 3H_2\,(g) \leftrightharpoons CH_3OH\,(l) + H_2O\,(l)$ | −49.5 | −9.04 |
| $CO_2\,(g) + H_2\,(g) \leftrightharpoons HCOOH\,(l)$ | −31.2 | 32.9 |
| $CO_2\,(g) + 4H_2\,(g) \leftrightharpoons CH_4\,(g) + 2H_2O\,(l)$ | −252.9 | −130.8 |
| $CO_2\,(g) + H_2\,(g) \leftrightharpoons CO\,(g) + H_2O\,(l)$ | 41.2 | −20.1 |

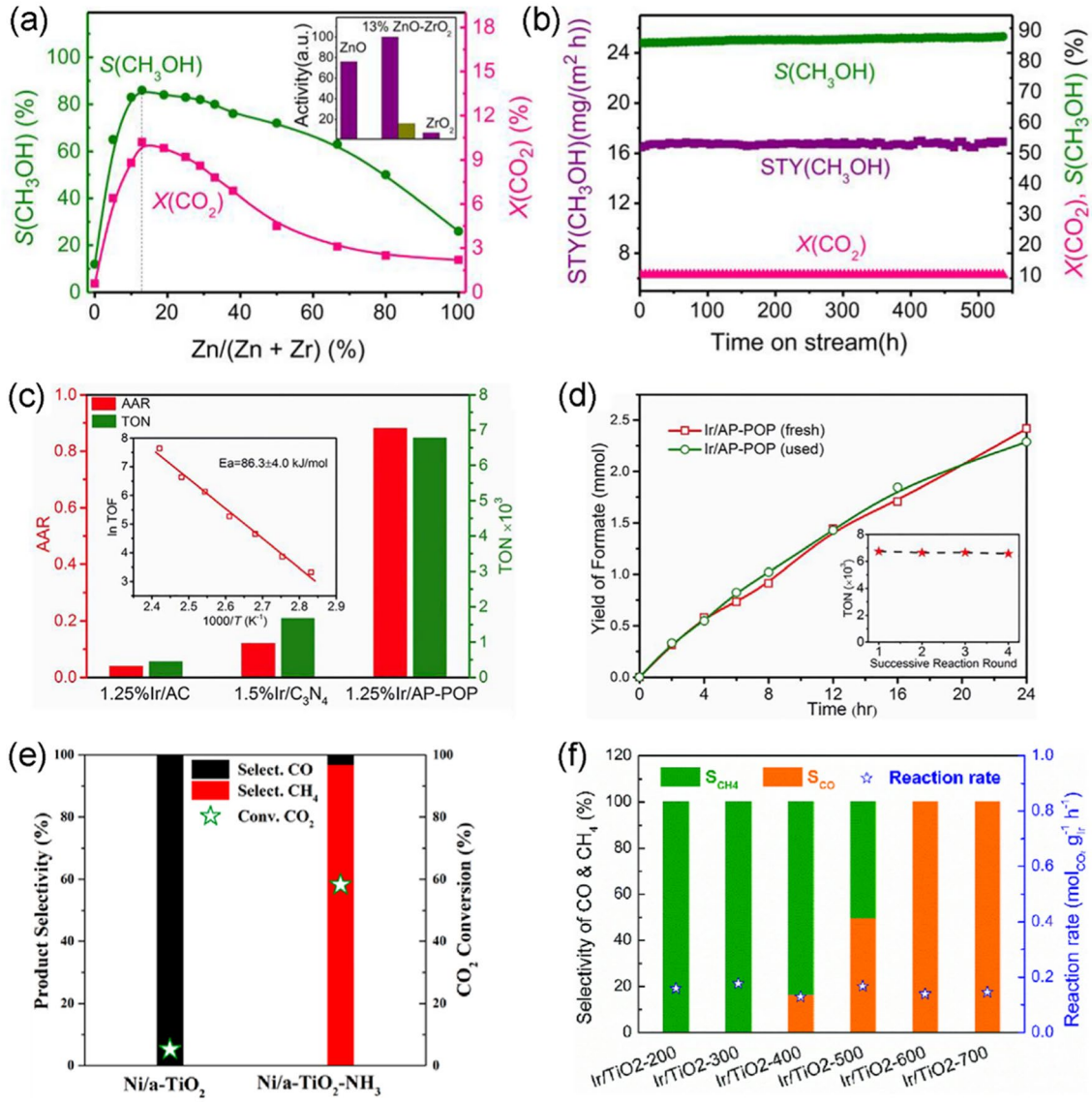


**Fig. 2** **a** Catalytic performance and **b** stability of $CO_2$ hydrogenation to methanol over the ZnO–$ZrO_2$ solid solution catalyst. Reproduced with permission from Ref. [22]. Copyright 2017, American Association for the Advancement of Science. **c** Catalytic performance and **d** stability of $CO_2$ hydrogenation to formate over the Ir/AP-POP catalyst. Reproduced with permission from Ref. [28]. Copyright 2019, Cell Press. **e** $CO_2$ methanation performance of Ni/a-$TiO_2$ and Ni/a-$TiO_2$-$NH_3$. Reproduced with permission from Ref. [37]. Copyright 2019, American Chemical Society. **f** $CO_2$ methanation performance of Ir/$TiO_2$ reduced at different temperatures. Reproduced with permission from Ref. [40]. Copyright 2020, Royal Society of Chemistry

proposed a revised route for direct hydrogenation of $CO_2$ to formate using a Schiff-base-modified Au catalyst, with a turnover number (TON) of 14 470 at 90 °C and 8 MPa. The in situ DRIFTS and density functional theory (DFT) calculation results indicated an unusual $CO_2$ activation pathway involving a weakly bonded carbamate zwitterion intermediate formed through the Lewis base adduct of $CO_2$. However, this reaction pathway only occurred with hydrogen lacking a Lewis base center in a polar solvent, such as water and methanol, used in this work. Huang and coworkers [28] further applied atomically dispersed catalysts to $CO_2$ hydrogenation to formate. A single Ir atom catalyst was prepared using a porous organic polymer with aminopyridine functionalities. It exhibited excellent performance for formate production, with a TON as high as 6784 at 120 °C and 8 MPa (Fig. 2c). Recycling experiments indicated that the catalytic activity did not decrease even after four uses (Fig. 2d). The catalytic mechanism was similar to that of a homogeneous mononuclear Ir pincer complex catalyst.

### Methane and CO

$CO_2$ hydrogenation to methane (methanation) and CO (RWGS) are usually two parallel processes, depending on the catalytic materials and reaction conditions. The produced methane via $CO_2$ methanation can serve as the principal component of synthetic natural gas, whereas the produced CO via RWGS can be integrated into syngas conversion systems [29]. Extensive studies on catalysis have been devoted to controlling selectivity toward methane versus CO at a considerable $CO_2$ conversion for given applications [30].

Among the metals (e.g., Ni, Ru, Rh, Pd, Ir, Co, Fe, and Cu) used for $CO_2$ methanation catalysts, Ni and Ru are the most active ones [30–33]. As non-noble metal catalysts, Ni-based catalysts hold great promise for practical methanation application. However, catalytically active Ni species are prone to sintering and deactivation because $CO_2$ methanation is a strongly exothermic reaction. An important strategy for dealing with this issue is to modulate the strong metal–support interaction (SMSI) between Ni NPs and oxides [34–39]. Pan and coworkers [37] determined that $CO_2$ methanation performance was remarkably suppressed and CO was the only product when Ni NPs were supported by conventional anatase (a-$TiO_2$) because of the SMSI-induced formation of a reduced $TiO_x$ overlayer around the Ni NPs at high temperature (500 °C). By contrast, pretreating the a-$TiO_2$ support with $NH_3$ and $H_2$ switched the selectivity from CO to methane with one order of magnitude increase in $CO_2$ conversion (Fig. 2e). The reduction pretreatments generated a large amount of $Ti^{3+}$ species in the a-$TiO_2$ support, which could weaken the SMSI and suppress the formation of the $TiO_x$ overlayer, leading to more Ni surface sites accessible to the reactants. As SMSI was first widely recognized for Pt group metals on reducible oxide supports, the growth of the $TiO_x$ overlayer was also observed in $TiO_2$-supported Ru and Ir NP catalysts for $CO_2$ methanation [32, 40, 41]. Huang and coworkers [40] demonstrated the increase of the grown $TiO_x$ overlayer around Ir NPs with the increase in the reduction pretreatment temperature, along with the selectivity shift from methane to CO (Fig. 2f). Recently, Fu and coworkers reported the growth of a $MoO_{3-x}$ layer over Ru NPs in $CO_2$ hydrogenation reaction gas and at a low temperature (250 °C), but its selectivity followed the aforementioned trend that the presence of an oxide layer overturned the major product from methane to CO, with the selectivity of both being close to unity [42].

As discussed previously, CO production via RWGS is also likely even with the most active methanation catalysts (e.g., Ni and Ru). Huang and coworkers [43] theoretically investigated the origin of such selectivity changes. They demonstrated that the C–O bond scission of the main intermediates (e.g., HCOO–, –COOH, and M–CO) was a key factor that determined methane/CO selectivity, which was correlated with the difference between the dissociation barrier and the desorption energy of metal carbonyls. With this knowledge, one can improve CO selectivity by decreasing the coordination number of supported metals or using metals at the lower right corner of the transition metal series. This theory likely explains the preferred formation of CO versus methane over $TiO_2$-supported metals with low loadings [43, 44] and Au-based catalysts [45].

## $CO_2$ Hydrogenation to $C_{2+}$ Products

The synthesis of $C_{2+}$ products with two or more carbon atoms from direct $CO_2$ hydrogenation via C–C coupling and carbon chain growth is attractive, as these products have a high energy density and can be used as basic chemicals for polymer synthesis or liquid fuels for transportation. Similar to CO hydrogenation, $CO_2$ hydrogenation also suffers from low selectivity toward specific $C_{2+}$ products [46–49]. Here, we discuss selective $CO_2$ hydrogenation to several subgroups of $C_{2+}$ products, including light olefins, aromatics, gasoline, and higher alcohols (e.g., ethanol). Because the pathway involved in the growth of the carbon chain for any given $C_{2+}$ product contains many successive reaction steps, tandem catalysis, which utilizes more than one catalyst to promote two or more mechanistically distinct reaction steps [50], has been used as a promising strategy for achieving high selectivity.

### Light Olefins

Light olefins ($C_2^=$–$C_4^=$), including ethylene, propylene, and butylene, are essential chemicals for the production of polymer materials, which are conventionally produced from steam cracking of naphtha and dehydrogenation of light alkanes. Light olefins can also be produced from $CO_2$ hydrogenation via a modified Fischer–Tropsch synthesis (FTS) pathway. However, the selectivity of $C_2$–$C_4$ hydrocarbons (including olefins and paraffins) is limited by the Anderson–Schulz–Flory (ASF) distribution (typically < 58%) [29]. For instance, modifying FTS catalysts (e.g., Fe) with structural and electronic promoters (e.g., Na and Mn) can only achieve a selectivity of < 50% for light olefins in hydrocarbons at a $CO_2$ conversion of approximately 40% [51, 52]. Thus, obtaining high selectivity toward light olefins while suppressing the production of alkane and CO (via RWGS) from $CO_2$ hydrogenation is challenging.

A concept of catalyst design for a bifunctional oxide–zeolite system proposed by Bao and coworkers [53] has been demonstrated to effectively surpass the ASF distribution limit. This concept is also applicable to $CO_2$ hydrogenation. Pan and coworkers [54] reported a bifunctional catalyst composed of ZnO–$Y_2O_3$ oxide and SAPO-34 zeolite, which achieved selective $CO_2$ hydrogenation to light olefins with

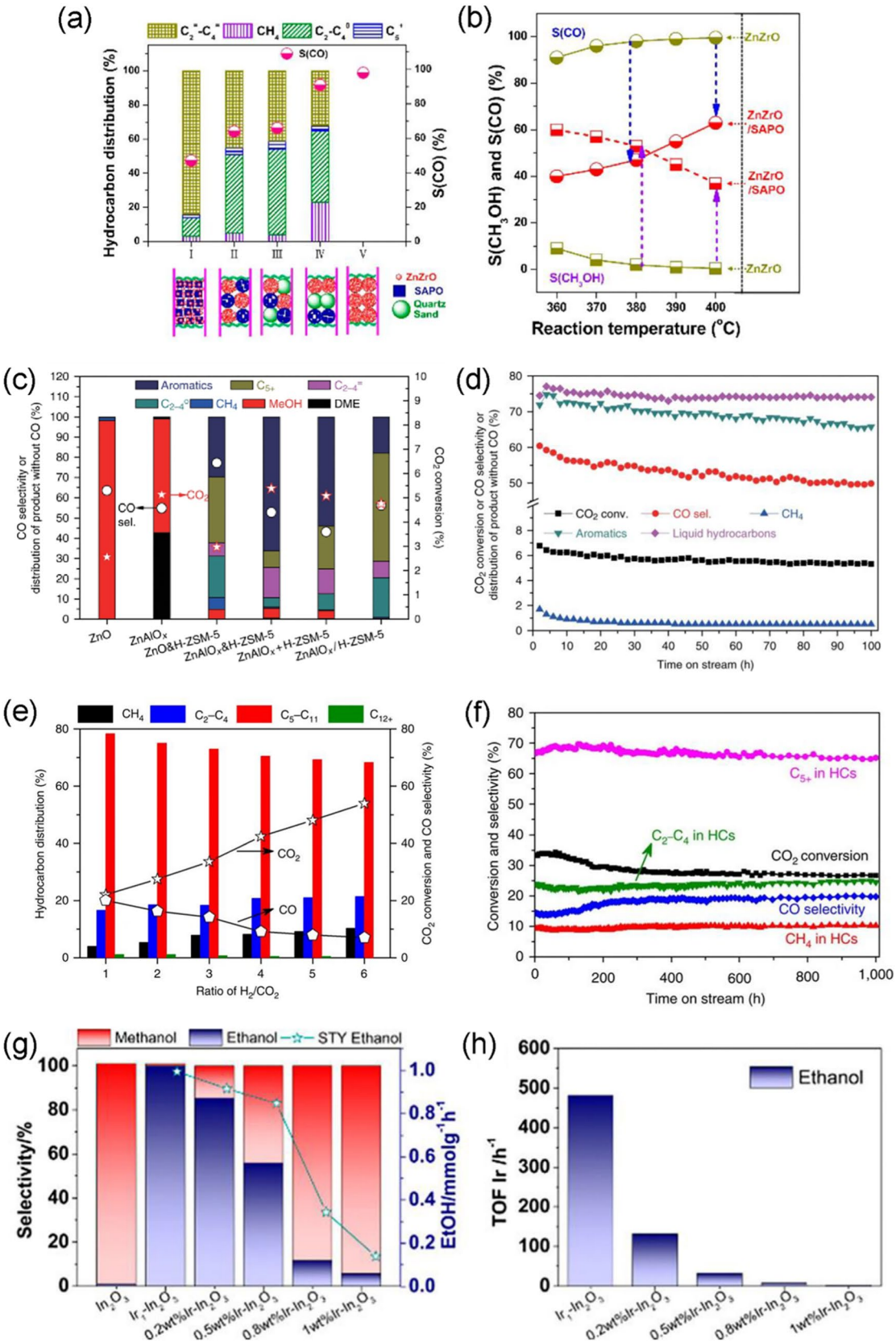
(a)
Hydrocarbon distribution (%)
S(CO) (%)
S(CO)
ZnZrO
SAPO
Quartz Sand
(b)
S(CO)
S(CH3OH) and S(CO) (%)
ZnZrO
ZnZrO /SAPO
ZnZrO /SAPO
ZnZrO
S(CH3OH)
Reaction temperature (°C)
(c)
Aromatics
MeOH
DME
CH4
CO sel.
CO2
CO selectivity or distribution of product without CO (%)
CO2 conversion (%)
ZnO
ZnAlOx
ZnO&H-ZSM-5
ZnAlOx&H-ZSM-5
ZnAlOx+H-ZSM-5
ZnAlOx/H-ZSM-5
(d)
CO2 conv.
CO sel.
CH4
Aromatics
Liquid hydrocarbons
CO2 conversion or CO selectivity or distribution of product without CO (%)
Time on stream (h)
(e)
CH4
C2–C4
C5–C11
C12+
CO2
CO
Hydrocarbon distribution (%)
CO2 conversion and CO selectivity (%)
Ratio of H2/CO2
(f)
C5+ in HCs
C2–C4 in HCs
CO2 conversion
CO selectivity
CH4 in HCs
Conversion and selectivity (%)
Time on stream (h)
(g)
Methanol
Ethanol
STY Ethanol
Selectivity/%
EtOH/mmolg-1h-1
In2O3
Ir1-In2O3
0.2wt%Ir-In2O3
0.5wt%Ir-In2O3
0.8wt%Ir-In2O3
1wt%Ir-In2O3
(h)
Ethanol
TOF Ir /h-1
Ir1-In2O3
0.2wt%Ir-In2O3
0.5wt%Ir-In2O3
0.8wt%Ir-In2O3
1wt%Ir-In2O3

◂**Fig. 3** **a, b** Performance of $CO_2$ hydrogenation to light olefins over the ZnZrO/SAPO tandem catalyst. Reproduced with permission from Ref. [55]. Copyright 2017, American Chemical Society. **c** Catalytic performance and **d** stability of $CO_2$ hydrogenation to aromatics over the $ZnAlO_x$/H-ZSM-5 tandem catalyst. Reproduced with permission from Ref. [56]. Copyright 2018, Springer Nature. **e** Catalytic performance and **f** stability of $CO_2$ hydrogenation to gasoline over the Na-$Fe_3O_4$/HZSM-5 multifunctional catalyst. Reproduced with permission from Ref. [62]. Copyright 2017, Springer Nature. **g, h** Performance of $CO_2$ hydrogenation to ethanol over the bifunctional $Ir_1$-$In_2O_3$ single-atom catalyst. Reproduced with permission from Ref. [64]. Copyright 2020, American Chemical Society

a selectivity of 83.9% in hydrocarbons at a $CO_2$ conversion rate of 27.6% at 390 °C. Li and coworkers [55] developed a ZnZrO/SAPO tandem catalyst composed of ZnO–$ZrO_2$ solid solution and Zn-modified SAPO-34 zeolite. With this catalyst, light olefins were produced from $CO_2$ hydrogenation with a selectivity as high as over 80% in hydrocarbons and a suppressed CO selectivity of 47% at a $CO_2$ conversion rate of 12.6% at 380 °C (Fig. 3a, b). The tandem catalysis mechanism involved the formation of $CH_xO$* species via $CO_2$ hydrogenation over the ZnO–$ZrO_2$ solid solution and the transformation of migrated $CH_xO$* species to light olefins over the Zn-modified SAPO-34 zeolite.

### Aromatics

Aromatics ($C_nH_{2n-6}$) are compounds that contain at least one benzene ring. Benzene, toluene, and xylenes of aromatic compounds are important bulk chemicals. Generally, aromatics are industrially derived from petroleum. Liu and coworkers [56] proposed a route for the synthesis of aromatics directly from $CO_2$ hydrogenation. They reported a $ZnAlO_x$/H-ZSM-5 catalyst with an aromatic selectivity of 73.9% and a low methane selectivity of 0.4% among carbon products (excluding CO) at a $CO_2$ conversion rate of 9.1% (Fig. 3c). This catalyst also showed good stability during a test for 100 h (Fig. 3d). Mechanistic studies indicated that methanol and dimethyl ether were formed via hydrogenation of formate species over $ZnAlO_x$ sites, migrated to H-ZSM-5 sites, and subsequently converted into olefins and aromatics. When replacing H-ZSM-5 with Si-H-ZSM-5 in the tandem catalyst, 58.1% p-xylene in xylenes could be achieved. Li and coworkers [57] developed a ZnZrO/ZSM-5 tandem catalyst, which achieved an aromatic selectivity of 73% at a $CO_2$ conversion rate of 14% and a suppressed CO selectivity of 44%. Sun and coworkers [58] combined a Na-$Fe_3O_4$ $CO_2$-FTS catalyst with ZSM-5 zeolites with rich Brønsted acid sites as a tandem catalyst for $CO_2$ hydrogenation to aromatics. This catalyst achieved a selectivity of 75% for light aromatics, and p-xylene accounted for as high as 72% of xylenes. A tandem catalysis process comprising $CO_2$ methanation and methane aromatization with two connected reactors [59] was also demonstrated for $CO_2$ hydrogenation to aromatics, with a benzene production rate of 0.68 μmol/(g min) at a high $CO_2$ conversion rate of 92%.

### Gasoline

Long-chain hydrocarbons in the gasoline range ($C_5$–$C_{11}$) can also be produced via direct $CO_2$ hydrogenation. Using this route, Sun and coworkers [60–63] conducted numerous studies using multifunctional composite catalysts composed of $CO_2$-FTS catalysts and zeolites. They developed a Na-$Fe_3O_4$/HZSM-5 catalyst that could achieve direct $CO_2$ conversion into gasoline with a selectivity of up to 78% in hydrocarbons and only a small amount of methane (4%) at a $CO_2$ conversion rate of 22% under industrially relevant conditions (Fig. 3e) [60]. Three types of active sites ($Fe_3O_4$, $Fe_5C_2$, and acid sites) at appropriate proximity to the multifunctional catalyst cooperatively catalyzed the tandem and synergetic catalytic conversion of $CO_2$ into long-chain gasoline fractions. The multifunctional catalyst also showed remarkable stability for 1000 h and held great promise as a potential industrial catalyst for $CO_2$ conversion into liquid fuels (Fig. 3f). Recently, Sun and coworkers further combined the Na-$Fe_3O_4$ $CO_2$-FTS catalyst with two zeolites (SAPO-11 and ZSM-5) in single-bed, dual-bed, and triple-bed arrangements for the production of gasoline with a high fraction of multibranched isoparaffins [62]. The triple-bed configuration composed of Na-$Fe_3O_4$, SAPO-11, and ZSM-5 achieved a gasoline selectivity of 71.7% in hydrocarbons at a $CO_2$ conversion rate of 31.2%, with an isoparaffin selectivity as high as 38.2%, corresponding to a research octane number (RON) value of 91.7.

### Ethanol

$CO_2$ conversion into ethanol has been realized using modified methanol synthesis or FTS catalysts. Over alkali-metal-modified methanol catalysts, methanol production is still high, leading to unsatisfactory ethanol selectivity. Over modified Fe-based or Co-based FTS catalysts, alcohol production follows the ASF distribution with a typical ethanol selectivity of approximately 35%. Thus, achieving high ethanol selectivity remains a challenge. Huang and coworkers [64] designed a bifunctional $Ir_1$–$In_2O_3$ single-atom catalyst, which showed an excellent ethanol selectivity of > 99% and an initial turnover frequency (TOF) of 481 $h^{-1}$ (Fig. 3g, h). Characterizations and DFT calculations indicated that isolated Ir sites in combination with adjacent oxygen vacancies forming Lewis acid–base pairs could activate $CO_2$ to produce *CO intermediates over Ir sites. By contrast, $In_2O_3$ was an active catalyst for methanol synthesis and produced $CH_3O$* intermediates. Ethanol could be formed over this bifunctional single-atom catalyst by coupling *CO and $CH_3O$* adjacent sites. Recently,

Huang and coworkers [65] developed a $K_{0.2}Rh_{0.2}/\beta$-$Mo_2C$ single-atom catalyst, which exhibited an ethanol selectivity of 72.1% at 150 °C.

### Other $CO_2$ Conversion Routes

Apart from hydrogenation, $CO_2$ can also be converted and utilized through other important routes. The dry reforming of methane with $CO_2$ provides an attractive route to simultaneously convert the two greenhouse gases into syngas [66]. Current studies mainly focus on the stability issue at a high reaction temperature, for instance, developing robust Ru/$MgAl_2O_4$ and Ni/h-BN catalysts [67, 68]. As a weak oxidant, $CO_2$ is also able to assist the dehydrogenation of light alkanes, including ethane, propane, and isobutane, during which $CO_2$ is reduced to CO [69–71]. Thermochemical splitting of $CO_2$ into CO and $O_2$ utilizing concentrated solar energy is also a promising route for $CO_2$ reduction [72]. The catalytic function of metal species (e.g., $IrO_x$ and Pd) that can activate $CO_2$ is still necessary in the $CO_2$ splitting reaction even at high temperatures [73, 74]. Some nonreductive $CO_2$ conversion routes can also produce valuable fine chemicals, such as organic carbonates [75, 76], cyclic carbonates [77–80], carboxylic acids [81, 82], and amides, via the N-formylation reaction [83].

## Electrocatalytic $CO_2$ Conversion

The conversion of $CO_2$ into chemicals and fuels via electrocatalysis can directly couple $CO_2$ utilization and the storage of renewable energy. Although the co-conversion of $CO_2$ with other molecules (e.g., $N_2$) has also been demonstrated [84], currently, the main electrocatalytic conversion route is still electrocatalytic $CO_2$ reduction or $CO_2$ electrolysis [85]. Here, it should be noted that there is no strict difference between $CO_2$ electroreduction and $CO_2$ electrolysis. $CO_2$ electroreduction is usually preferred by the catalysis community, whereas $CO_2$ electrolysis is often used by the electrochemistry community. Rather than using $H_2$ produced by water electrolysis in thermocatalytic $CO_2$ hydrogenation reactions, the electrocatalytic $CO_2$ reduction reaction utilizes active hydrogen species directly derived from water activation to achieve the reduction of $CO_2$. Compared with thermal catalysis, it can drive electrocatalytic $CO_2$ reduction under mild conditions, e.g., room/low temperatures (< 100 °C) and ambient pressures. By contrast, high-temperature $CO_2$ electrolysis is used in some application scenarios, such as $O_2$ production for space missions on Mars in the 1960s and direct electrolysis of high-temperature flue gas containing highly concentrated $CO_2$.

### High-Temperature $CO_2$ Electrolysis to CO and Syngas

Figure 4a shows the energy demand for $CO_2$ electrolysis to CO ($CO_2 \rightarrow CO + 1/2O_2$) at different temperatures [86]. As the enthalpy change ($\Delta H$) is constant regardless of temperature, the electrical energy demand ($\Delta G$) decreases, whereas the heat demand ($T\Delta S$) increases with the increase in the reaction temperature. Therefore, a high-temperature $CO_2$ electrolysis process heated with industrial waste heat and Joule heat inside an electrolysis cell can effectively lower the electrical energy consumption. Thermodynamic analysis indicates that the formation of CO and/or syngas becomes more favorable at high temperatures compared with other $CO_2$ reduction products. High-temperature $CO_2$ electrolysis is usually conducted in solid oxide electrolysis cells (SOECs) using oxygen-ion-conducting or proton-conducting solid oxides as electrolytes at high operating temperatures (up to 1000 °C). Different electrode reactions occur at cathodes and anodes when oxygen ions or protons are used as ion carriers. SOECs using proton-conducting electrolytes can work at low-to-intermediate temperatures (400 to 700 °C), at which reduced products, such as hydrocarbons, can also be generated from the point of view of thermodynamics. Because of the poor stability of proton-conducting electrolytes under $CO_2$ electrolysis conditions, to date, most studies have been conducted using oxygen-ion-conducting SOECs [87, 88]. When $CO_2$ and water are co-fed to SOECs, the final product can be syngas with different $H_2$/CO ratios, even hydrocarbons (e.g., methane and ethylene) with the aid of other metal catalysts for syngas conversion [88, 89].

The state-of-the-art cathode material for $CO_2$ electrolysis in SOECs is yttria-stabilized zirconia-supported Ni (Ni/YSZ). However, the Ni/YSZ cathode suffers from carbon deposition, grain coarsening, and Ni oxidation under the reaction conditions (i.e., $CO_2$ atmosphere and high temperature), leading to poor stability [90, 91]. Recently, mixed ionic and electronic conductors, such as perovskite oxides ($ABO_3$), have been used as alternative cathode materials because of their good redox stability and high carbon deposition resistance; however, they show inferior $CO_2$ electrolysis performance compared with the Ni/YSZ cathode. The performance of perovskite oxides has been improved by element doping [92–96], anchoring single-metal sites on the surface [97], constructing catalytically active oxide–oxide interfaces via infiltration [98, 99] and metal–oxide interfaces via metal decoration [100], and in situ exsolution of metal NPs [101–104]. The in situ exsolution treatment can produce many metal–alloy NPs (e.g., Rh, Pd, Pt, Fe, Ni, Co, FeNi, CoFe, and RuFe) on perovskite surfaces under reducing environments; however, the number of NPs is low because of the sluggish diffusion of B-site dopant cations in the bulk perovskite. Through repeated redox treatments, Wang and coworkers [104] promoted the exsolution of RuFe

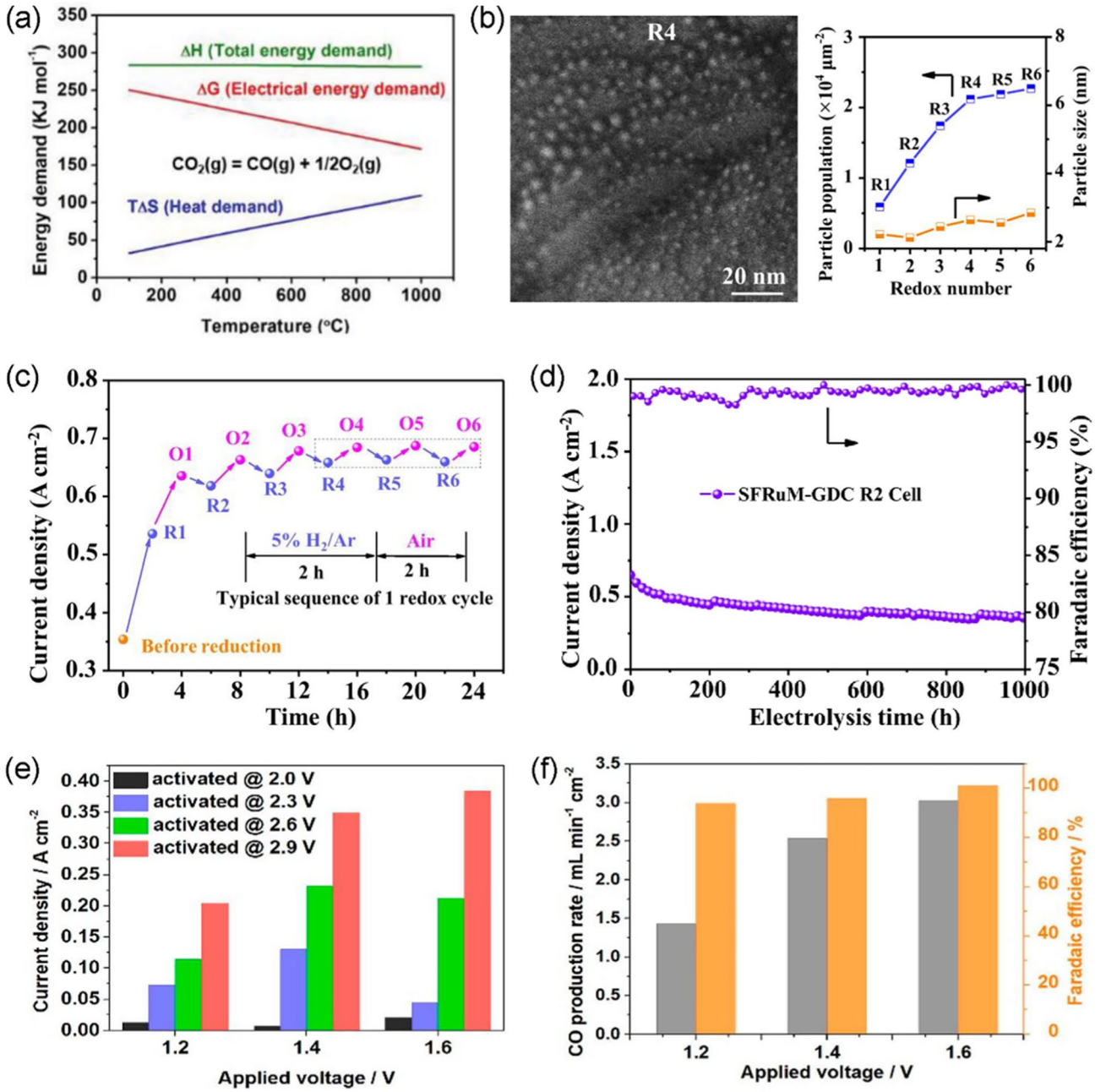


**Fig. 4** **a** Temperature dependence of energy demand for $CO_2$ electrolysis to CO ($CO_2 \rightarrow CO + 1/2O_2$). Reproduced with permission from Ref. [86]. Copyright 2019, Wiley–VCH. **b** Density and size of RuFe alloy NPs on SFRuM perovskite surfaces. **c** $CO_2$ electrolysis performance and **d** stability of SFRuM after redox treatments. Reproduced with permission from Ref. [104]. Copyright 2021, Wiley–VCH. **e** $CO_2$ electrolysis current density and **f** electrochemical impedance spectroscopy at 1.4 V. Reproduced with permission from Ref. [105]. Copyright 2021, American Chemical Society

alloy NPs on $Sr_2Fe_{1.4}Ru_{0.1}Mo_{0.5}O_{6-\delta}$ (SFRuM) perovskite. The dynamic exsolution and redissolution processes of the RuFe alloy NPs were imaged by in situ secondary electron scanning transmission electron microscopy at 600 to 850 °C in a 10-Pa $H_2$ or $O_2$ atmosphere. The density of exsolved RuFe alloy NPs was as high as approximately 21,000 $\mu m^{-2}$ after four redox cycles, whereas the NP size did not change (Fig. 4b). The in situ grown RuFe@SFRuM interface after four redox cycles increased the current density of $CO_2$ electrolysis (approximately 0.65 A/cm$^2$) by 74.6% and contributed to high stability for 1000 h at 1.2 V and 800 °C (Fig. 4c, d). Zhu and coworkers [105] reported the in situ dispersion of an Au layer used as a current collector to Au NPs (down to 2 nm) at 800 °C by applying high cell voltages. During

this transformation, Au/YSZ was reconstructed into nano-Au/Zr–suboxide interfaces, which resulted in a decrease in the polarization resistance by a factor of 75, along with a 38-fold improvement in $CO_2$ electrolysis current density (Fig. 4e, f).

## Low-Temperature Electrocatalytic $CO_2$ Reduction

Low-temperature electrocatalytic $CO_2$ reduction occurs at room temperature to low temperature (< 100 °C) using liquid water and/or vapor as a reactant. Table 2 lists the standard potentials of $CO_2$ electroreduction for various products. The $CO_2$ electroreduction reaction is thermodynamically not that difficult, but it is hindered by the hydrogen evolution reaction (HER). Moreover, $CO_2$ electroreduction involves multiple proton and electron transfer steps, leading to highly complex reaction pathways toward a variety of products, including CO, formic acid (formate), methane, methanol, ethylene, ethanol, acetate acid (acetate), and *n*-propanol. Therefore, selectivity control is a core aspect of $CO_2$ electroreduction studies, particularly for reduced and $C_{2+}$ products. In terms of practical applications, high selectivity toward given products should be obtained at an industrial current density, with considerable stability.

### Electrocatalytic $CO_2$ Reduction to CO and Formic Acid (Formate)

CO and formate are the most widely reported $C_1$ products from $CO_2$ electroreduction. Although Hori's seminal works [106, 107] in the 1980s have classified bulk metals into several groups in terms of major products, such as CO, formate, hydrocarbons, or $H_2$, remarkable differences can be observed in nanostructured metal catalysts [108–117]. For instance, Pd is an active metal for HER, and bulk Pd mainly produces $H_2$ in $CO_2$ electroreduction; however, Pd NPs show impressive performance for $CO_2$ electroreduction to CO or formate, both with a Faradaic efficiency of > 90%, depending on the applied electrode potentials (Fig. 5a). This selectivity switch can be rationalized by potential-induced and intermediate-induced active phase transition under the reaction conditions [8, 118, 119]. The CO production over Pd NPs can be further improved by alloying Pd with second metals [120, 121]. Notably, the electrochemical promotion of the catalysis effect was also observed in $CO_2$ hydrogenation to formate over Pd NPs in the liquid phase under ambient conditions [122]. Inspired by the concept of nanoconfinement catalysis proposed by Bao [10], Wang and coworkers [123] developed an Au(Ag)-$CeO_x$ catalyst with abundant metal–oxide interfaces. In situ scanning tunneling microscopy and X-ray photoemission spectroscopy results indicated that these interfaces enhanced $CO_2$ adsorption and hydrogenation to the initial *COO and *COOH intermediates, thus leading to high Faradaic efficiency and partial current density for CO production (Fig. 5b). Another important example is using single Ni atom catalysts [124–132] instead of Ni bulk or NPs that are good HER catalysts. Wang and coworkers [124] developed nickel–nitrogen (Ni–N) sites embedded within porous carbon with a Ni loading of up to 5.44 wt% through pyrolysis of Zn/Ni bimetallic zeolitic imidazolate framework-8. This catalyst achieved a high CO current density of 71.5 mA/cm$^2$, corresponding to a TOF of 10,087 h$^{-1}$ with a CO Faradaic efficiency of more than 92% in an H-cell (Fig. 5c, d). The atomically dispersed Ni–N sites are coordinatively unsaturated and can suppress the HER [125]. Heteroatom-doped carbon materials have also been used for $CO_2$ electroreduction to CO [133–135]. Apart from the catalysts themselves, the reaction conditions, such as electrolyte composition and temperature, also play important roles in determining selectivity [136–138].

In addition to the unique Pd catalysts [8, 118, 119], formate can also be produced using a series of catalysts, such as Bi, Sn, and Pb compounds [139–143], Cu alloy with Sn and In [144–146], and single-atom alloy catalysts [147]. Wang and coworkers [144] reported an in situ reconstructed hierarchical Sn-Cu/$SnO_x$ core/shell ($Sn_{2.7}Cu$) catalyst, which achieved a current density of 406.7 mA/cm$^2$ at − 0.70 V versus reversible hydrogen electrode (RHE) and high stability at 243.1 mA/cm$^2$ for 40 h at − 0.55 V versus RHE in a flow cell. Xiao and coworkers [147] developed a single-atom Pb-alloyed Cu catalyst ($Pb_1Cu$) that can exclusively convert $CO_2$ into formate with approximately 96% Faradaic efficiency at more than 1 A/cm$^2$. Formate production occurred over the modulated Cu sites rather than the isolated Pb sites in the $Pb_1Cu$ catalyst, following an HCOO* pathway. The production of a pure formic acid solution at 100 mA/cm$^2$ for 180 h was further demonstrated with the $Pb_1Cu$ catalyst in a 3-cm$^2$ electrode device using a proton-conducting solid electrolyte.

**Table 2** Standard potentials of $CO_2$ electroreduction to various products at pH = 0

| Reaction | $E^o$ (V vs. SHE) |
|---|---|
| $CO_2 + 2H^+ + 2e^- \rightarrow CO + H_2O$ | − 0.11 |
| $CO_2 + 8H^+ + 8e^- \rightarrow CH_4 + 2H_2O$ | 0.17 |
| $CO_2 + 6H^+ + 6e^- \rightarrow CH_3OH + H_2O$ | 0.016 |
| $2CO_2 + 12H^+ + 12e^- \rightarrow C_2H_4 + 4H_2O$ | 0.08 |
| $2CO_2 + 12H^+ + 12e^- \rightarrow C_2H_5OH + 3H_2O$ | 0.09 |
| $3CO_2 + 18H^+ + 18e^- \rightarrow n\text{-}C_3H_7OH + 5H_2O$ | 0.10 |

### Electrocatalytic $CO_2$ Reduction to Methane

Methane, as a fully reduced $C_1$ product, is usually produced using Cu catalysts at negative potentials [148]. However, some non-Cu catalytic materials can also reduce

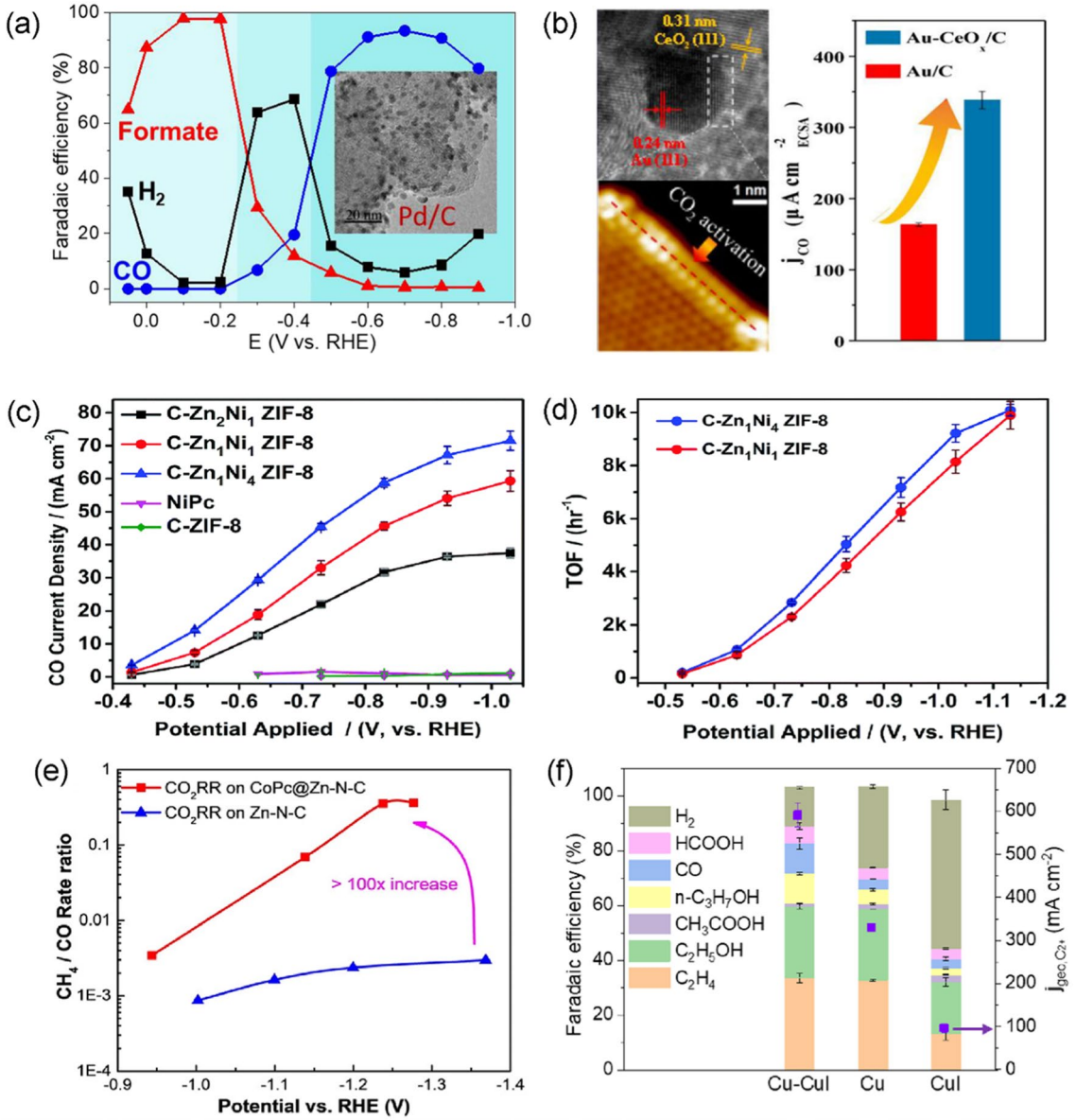


**Fig. 5** **a** Selectivity switch of $CO_2$ electroreduction over Pd/C catalysts. Reproduced with permission from Ref. [118]. Copyright 2017, Springer Nature. **b** Au–$CeO_x$ interface enhances $CO_2$ electroreduction. Reproduced with permission from Ref. [123]. Copyright 2017, American Chemical Society. **c, d** $CO_2$ electroreduction performance of Ni–N–C catalyst. Reproduced with permission from Ref. [124]. Copyright 2018, Royal Society of Chemistry. **e** $CO_2$ electroreduction performance of CoPc@Zn-N–C catalyst. Reproduced with permission from Ref. [149]. Copyright 2020, Wiley–VCH. **f** $CO_2$ electroreduction performance of Cu-CuI composite catalyst. Reproduced with permission from Ref. [161]. Copyright 2021, Wiley–VCH

$CO_2$ to methane. Wang and coworkers [149] demonstrated a cobalt phthalocyanine (CoPc) and zinc–nitrogen–carbon (Zn–N–C) tandem catalyst that can efficiently convert $CO_2$ into methane. The methane production rate of CoPc/Zn–N–C was over 100 times higher than that of CoPc or Zn–N–C alone (Fig. 5e). This catalyst decoupled complicated methane pathways over single active sites (for Cu catalysts) into a two-step tandem reaction. $CO_2$ was reduced to CO over CoPc; then, CO diffused onto Zn–N–C for further hydrogenation to methane.

## Electrocatalytic $CO_2$ Reduction to $C_{2+}$ Products

Compared with $C_1$ products, $C_{2+}$ products, such as ethylene, ethanol, and *n*-propanol, have higher energy density and broader availability. The formation of these products

involves C–C coupling, a key topic in fundamental catalysis research. More importantly, selectivity control after the C–C coupling step would determine the product distribution among $C_{2+}$ products [150–156]. The highly selective production of a specific single $C_{2+}$ product relies on the proper mechanistic understanding of full reaction pathways. The oxidation state of Cu has been considered to play a critical role in the formation of $C_{2+}$ products, with the $Cu^+$ species being the most catalytically active because of the presence of $Cu^0/Cu^+$ interfaces [157–160]. Wang and coworkers [161] designed a Cu–CuI composite catalyst with abundant $Cu^0/Cu^+$ interfaces by physically mixing commercial Cu NPs and CuI powders. This catalyst achieved a remarkable partial current density of 591 mA/cm$^2$ for $C_{2+}$ products at − 1.0 V versus RHE in a flow cell (Fig. 5f). The high-rate $C_{2+}$ generation was attributed to the presence of residual $Cu^+$ and adsorbed iodine species, which could facilitate CO adsorption and subsequent C–C coupling. Although the total $C_{2+}$ Faradaic efficiency could reach 71% at such a high current density, further efforts should be made to improve the selectivity toward a single $C_{2+}$ product, such as ethylene and ethanol.

## Tandem Catalysis Mechanism in Catalytic $CO_2$ Conversion Reactions

The selective generation of highly reduced products, such as hydrocarbons and oxygenate, via catalytic $CO_2$ conversion is not only desirable but also challenging because of multiple electron–proton transfer steps during these reactions. Tandem catalysis has been demonstrated as an emerging and promising strategy in $CO_2$ conversion into highly reduced products [162]. In principle, a tandem catalyst with two or more catalytically active sites is expected to break the linear scaling relationship of the adsorption of key intermediates, resulting in remarkably improved selectivity toward specific products [53]. As mentioned previously, Wang and coworkers [149] fabricated a CoPc/$ZnN_4$ tandem catalyst (Fig. 6a), in which $CO_2$ was reduced to CO over CoPc and the generated CO diffused onto the $ZnN_4$ site for subsequent hydrogenation to methane. This tandem effect is also applied to promote the formation of $C_2$ products (e.g., ethylene) when combining CO-producing sites with Cu sites into a single catalyst (Fig. 6b), for instance, Cu/Ag [163] and Cu/Ni–N–C [164]. In thermocatalytic $CO_2$ conversion, tandem catalysis plays a vital role in generating highly reduced and multicarbon products [54–57, 60, 165–167]. Generally, the oxide component of these tandem catalysts accounts for the formation of $C_1$ intermediates (e.g., *CO and *$CH_xO$), whereas the

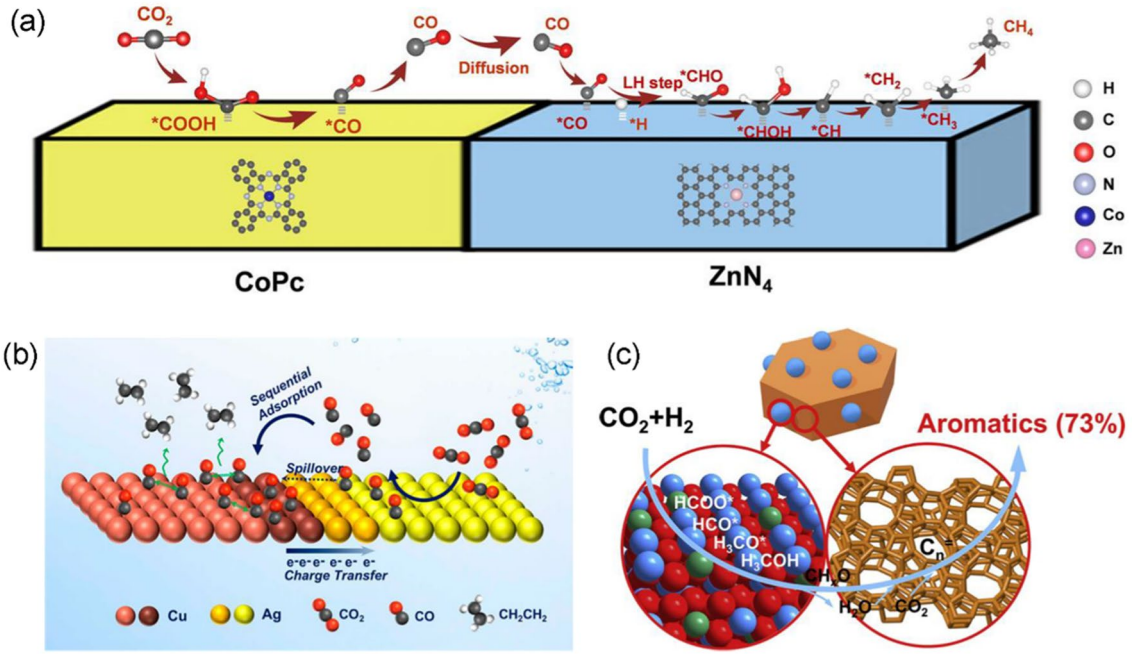


**Fig. 6** Proposed reaction mechanisms for $CO_2$ electroreduction to **a** methane over CoPc/$ZnN_4$ tandem catalyst and **b** ethylene over Cu/Ag tandem catalyst as well as **c** for $CO_2$ Hydrogenation to aromatics over ZnZrO/ZSM-5 tandem catalyst. **a** Reproduced with permission from Ref. [149]. Copyright 2020, Wiley–VCH. **b** Reproduced with permission from Ref. [163]. Copyright 2019, American Chemical Society. **c** Reproduced with permission from Ref. [57]. Copyright 2019, Cell press

zeolite component catalyzes C–C coupling to form light olefins, aromatics, gasoline, and higher alcohols (Fig. 6c).

## Development of $CO_2$ Electrolyzers at Industrial Current Densities

Beyond catalyst design, the rational design of efficient $CO_2$ electrolyzers is also of great importance for scaling up $CO_2$ electroreduction toward practical applications. The electrolyzers should be operated at industrial current densities (> 200 mA/cm$^2$), which could be achieved using the gas diffusion electrode configuration that breaks the limitation of $CO_2$ solubility. Flow and membrane electrode assembly (MEA) cells are the two main $CO_2$ electrolyzers [168, 169], of which MEA electrolyzers hold great promise because of their low iR drop, compact structure, improved stability, and high full cell energy efficiency (from electrical energy to chemical energy). With such electrolyzers, it is likely to only feed $CO_2$ and pure water as reactants without using any liquid electrolyte solution [170]. Wang and coworkers [171] developed a 4-cm$^2$ alkaline MEA $CO_2$ electrolyzer working at industrial current densities (Fig. 7a), which achieved a total Faradaic efficiency of 80% for $CO_2$ electroreduction over commercial Cu NPs at 350 mA/cm$^2$ with an energy efficiency of approximately 30% under optimized reaction conditions (Fig. 7b, c). The scale-up demonstration with a geometric electrode size of 100 cm$^2$ at the laboratory level has been achieved by Wang and coworkers. With the continuous technological improvement of the electrode structure, ion exchange membrane, and electrolyzer, current density ($CO_2$ reduction rate) and energy efficiency are expected to significantly increase [172]. To increase single-pass $CO_2$ conversion, large-area electrolyzers and stacks should be assembled, and this has been investigated by some groups [173].

Although the anion exchange membrane-based (alkaline) MEA electrolyzer holds great promise, it encounters a basic problem in low-temperature $CO_2$ electrolysis, i.e., carbonate formation [174, 175]. $CO_2$ reacts with surface $OH^-$ ions produced during electrolysis to form carbonate ($CO_3^{2-}$/$HCO_3^-$). Carbonate would precipitate in salt form to block catalyst surfaces, which reduces electrode hydrophobicity, leading to flooding. Moreover, carbonate can transfer to the anode through the anion exchange membrane, thereby leading to significant carbon loss and a low $CO_2$ utilization efficiency [176, 177]. Possible strategies for dealing with the carbonate issue are to use a cation exchange membrane, bipolar membrane, and solid electrolyte buffer layer [168,

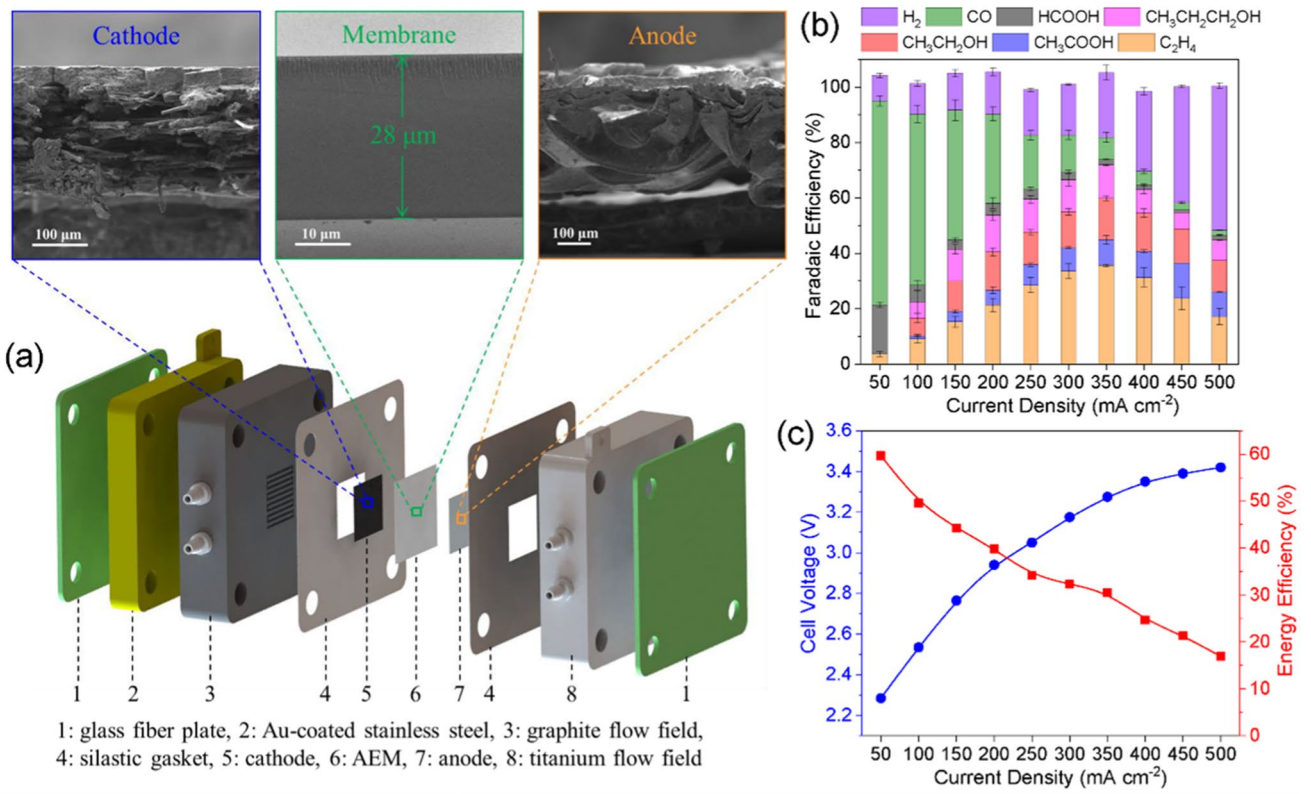


**Fig. 7** **a** Schematic of MEA $CO_2$ electrolyzer. **b, c** $CO_2$ electroreduction performance of Cu catalyst measured in MEA electrolyzer. Reproduced with permission from Ref. [171]. Copyright 2020, Springer Nature

169, 178–180]. This leads to an emerging direction, i.e., acid $CO_2$ electrolysis that has been demonstrated to suppress carbonate formation [181–184]. Moreover, the use of a two-step tandem conversion process, i.e., $CO_2$ electrolysis to CO in SOECs and CO electrolysis to $C_{2+}$ (e.g., ethylene and ethanol) in MEA electrolyzers, is feasible [185]. This tandem process also highlights the full use of individual advantages of high-temperature electrolysis (for the desired $CO_2$ activation) and low-temperature electrolysis (for the desired deep reduction of carbon intermediates). Another promising two-step $CO_2$–to–$C_{2+}$ conversion process is to connect an acidic MEA electrolyzer and an alkaline MEA electrolyzer in sequence, which combines the advantage of acidic $CO_2$ electrolysis (free of carbonate formation) and alkaline CO electrolysis (improved $C_{2+}$ production).

## Photo(electro)catalytic $CO_2$ Conversion

The conversion of $CO_2$ and water into chemicals and fuels via solar-driven photocatalysis and photoelectrocatalysis (PEC) with the aid of an efficient photocathode, which mimics the natural photosynthetic process, is generally known as artificial photosynthesis. The products of photocatalytic and PEC $CO_2$ reduction mainly include CO, methane, and ethylene [9, 186–189]. To date, semiconductor materials have been widely used to fabricate photocathodes for photocatalytic and PEC $CO_2$ reduction; however, the solar-to-fuel energy conversion efficiency is still unsatisfactory for practical applications. To improve the performance of photocatalytic/PEC $CO_2$ reduction, the construction of heterostructure photocathodes comprising multiple components is an important approach. Li and coworkers [190] developed an Au/p-GaN plasmonic heterostructure photocatalyst for selective and unassisted gas phase photocatalytic $CO_2$ reduction to CO under visible-light illumination. A metal/insulator/semiconductor configuration with a nanometer-thick aluminum oxide layer between Au/Cu NPs and p-GaN could remarkably improve the CO production rate (Fig. 8a). Zong and coworkers [191] reported a sandwich-like organic–inorganic hybrid perovskite-based photocathode for PEC $CO_2$ reduction to CO. The photocathode decorated with carbon encapsulation and a cobalt phthalocyanine molecular catalyst exhibited a high photocurrent density of − 15.5 mA/cm$^2$ at − 0.11 V versus RHE under air mass (AM) 1.5 G illumination with a stable CO Faradaic efficiency of more than 80% for 25 h (Fig. 8b). Unbiased PEC $CO_2$ reduction in tandem with an amorphous Si photoanode achieved a total solar-to-fuel energy conversion efficiency of 3.85%.

## Concluding Remarks

The recent progress in the conversion of $CO_2$ into valuable chemicals and fuels (e.g., CO, formic acid, methanol, methane, ethanol, acetic acid, propanol, light olefins, aromatics, and gasoline) via thermal catalysis, electrocatalysis, and photo(electro)catalysis has been reviewed, with an emphasize on highlighting some representative studies. The structure–performance correlations of typical catalysts used in these reactions have been revealed by combined advanced in situ spectroscopy and microscopy characterizations and DFT calculations. The control in activity, selectivity, and stability in future catalysis research at a fundamental level should aim at addressing issues facing practical applications. To reduce the cost of downstream separation and purification processes, catalytic selectivity toward a single $CO_2$ reduction product/fraction should be further improved at an industrially relevant $CO_2$ conversion rate with considerable stability in the future. Such selectivity control can be achieved by designing new catalytic materials and developing new $CO_2$ conversion routes with coupling multiple external fields (e.g., light, thermal, electrical, and magnetic). From the view of fundamental research, catalysts should be characterized in their working state during $CO_2$ conversion reactions using in situ/operando methods with high temporal and spatial resolutions and sufficient surface sensitivity to gain a proper understanding of their structure–performance correlations.

The scale-up of some catalytic $CO_2$ conversion routes has been demonstrated at the industrial level in China and around the world, e.g., the liquid sunshine demonstration project in Lanzhou, China, which synthesizes methanol from $CO_2$ hydrogenation coupled with photovoltaic-driven water electrolysis; the pilot project of direct $CO_2$ hydrogenation to gasoline in Jining, China; the high-temperature SOEC $CO_2$ electrolysis demonstration by the company of Haldor Topsøe; and low-temperature $CO_2$ electrolysis demonstration by the company Siemens. This exciting industrial progress encourages the research community to further join forces to scale-up other important catalytic $CO_2$ conversion routes, such as $CO_2$ hydrogenation to light olefins and aromatics and tandem $CO_2$ electrolysis ($CO_2$–CO–ethylene) in connected SOEC and MEA electrolyzers as well as connected acidic and alkaline MEA electrolyzers.

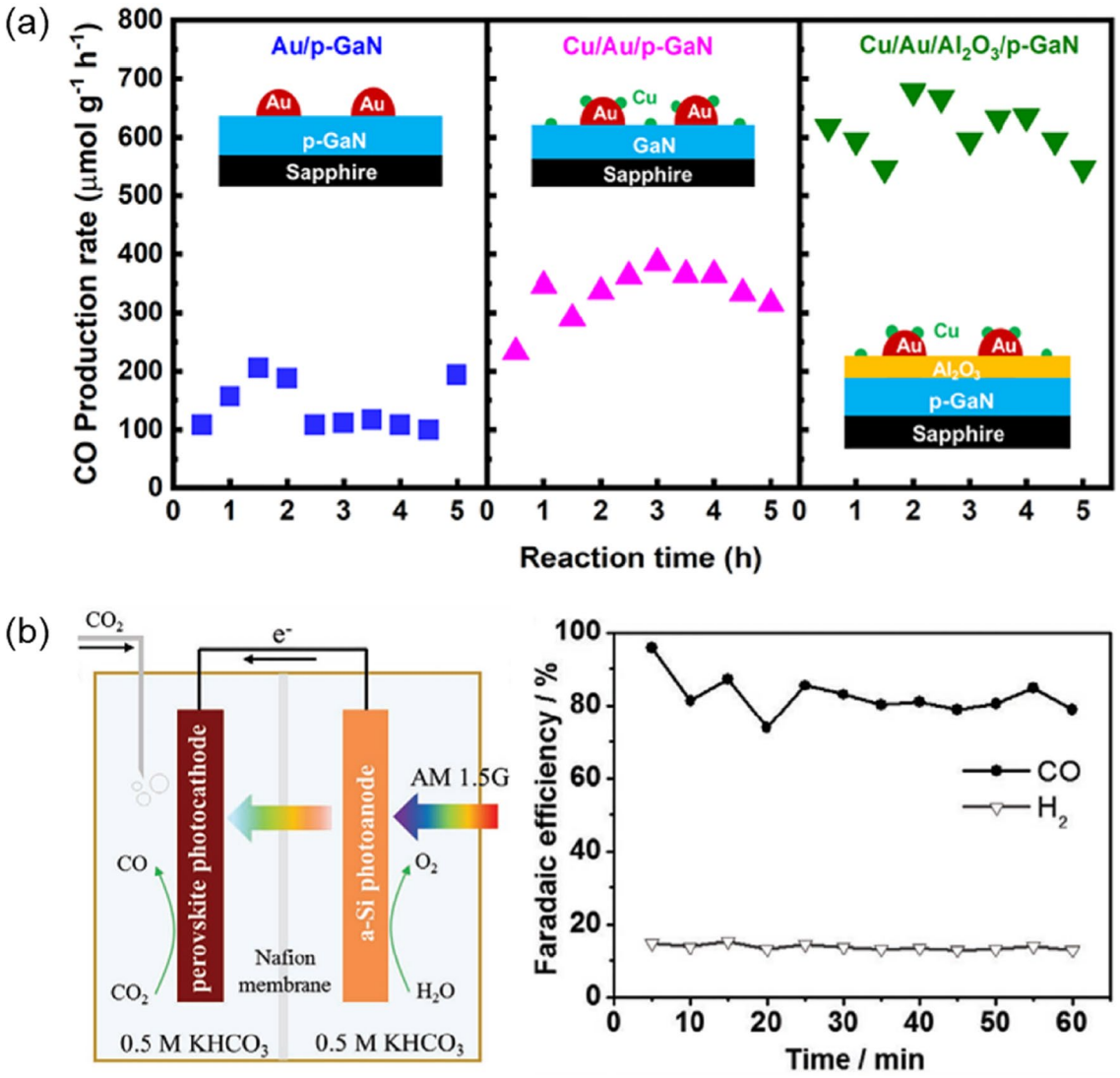


**Fig. 8** **a** Photocatalytic $CO_2$ reduction to CO production of Au/p-GaN, Cu/Au/pGaN, and Cu/Au/$Al_2O_3$/p-GaN samples under visible-light illumination. Reproduced with permission from Ref. [190]. Copyright 2021, American Chemical Society. **b** Faradaic efficiencies of CO and $H_2$ in unassisted PEC tandem system. Reproduced with permission from Ref. [191]. Copyright 2020, Wiley–VCH

**Acknowledgements** This work was supported by the National Key R&D Program of China (2021YFA1501503), the National Natural Science Foundation of China (Nos. 22002155, 22125205, 92045302), the Strategic Priority Research Program of the Chinese Academy of Sciences (XDB17020200), the CAS Youth Innovation Promotion (Y201938), the Natural Science Foundation of Liaoning Province (2021-MS-022) and the High-Level Talents Innovation Project of Dalian City (2020RQ038).

## Declarations

**Conflict of interest** The authors declare that they have no conflicts of interest.

## References


1. Artz J, Müller TE, Thenert K et al (2018) Sustainable conversion of carbon dioxide: an integrated review of catalysis and life cycle assessment. Chem Rev 118(2):434–504
2. Burkart MD, Hazari N, Tway CL et al (2019) Opportunities and challenges for catalysis in carbon dioxide utilization. ACS Catal 9(9):7937–7956
3. Tackett BM, Gomez E, Chen JG (2019) Net reduction of $CO_2$ via its thermocatalytic and electrocatalytic transformation reactions in standard and hybrid processes. Nat Catal 2(5):381–386
4. Ling YF, Ma QL, Yu YF et al (2021) Optimization strategies for selective $CO_2$ electroreduction to fuels. Trans Tianjin Univ 27(3):180–200
5. Gao P, Li SG, Bu XN et al (2017) Direct conversion of $CO_2$ into liquid fuels with high selectivity over a bifunctional catalyst. Nat Chem 9(10):1019–1024
6. Cai T, Sun HB, Qiao J et al (2021) Cell-free chemoenzymatic starch synthesis from carbon dioxide. Science 373(6562):1523–1527
7. Xu LY, Wang QX, Lin LW et al (1997) Production of light olefins from $CO_2$ hydrogenation over Fe/silicalite-2 catalysts I. Catalytic reactivity and reaction mechanism. J Nat Gas Chem 6(2):111–120
8. Gao DF, Zhou H, Wang J et al (2015) Size-dependent electrocatalytic reduction of $CO_2$ over Pd nanoparticles. J Am Chem Soc 137(13):4288–4291
9. Tang LQ, Chen RT, Meng XG et al (2018) Unique homoheterojunction synergistic system consisting of stacked BiOCl nanoplate/Zn-Cr layered double hydroxide nanosheets promoting photocatalytic conversion of $CO_2$ into solar fuels. Chem Commun 54(40):5126–5129
10. Yang F, Deng DH, Pan XL et al (2015) Understanding nano effects in catalysis. Natl Sci Rev 2(2):183–201
11. Su X, Yang XF, Huang YQ et al (2019) Single-atom catalysis toward efficient $CO_2$ conversion to CO and formate products. Acc Chem Res 52(3):656–664
12. Shih CF, Zhang T, Li JH et al (2018) Powering the future with liquid sunshine. Joule 2(10):1925–1949
13. Tian P, Wei YX, Ye M et al (2015) Methanol to olefins (MTO): from fundamentals to commercialization. ACS Catal 5(3):1922–1938
14. Liang BL, Ma JG, Su X et al (2019) Investigation on deactivation of $Cu/ZnO/Al_2O_3$ catalyst for $CO_2$ hydrogenation to methanol. Ind Eng Chem Res 58(21):9030–9037
15. Sha F, Han Z, Tang S et al (2020) Hydrogenation of carbon dioxide to methanol over non-Cu-based heterogeneous catalysts. Chemsuschem 13(23):6160–6181
16. Yu JF, Yang M, Zhang JX et al (2020) Stabilizing $Cu^+$ in $Cu/SiO_2$ catalysts with a shattuckite-like structure boosts $CO_2$ hydrogenation into methanol. ACS Catal 10(24):14694–14706
17. Wang WW, Qu ZP, Song LX et al (2020) $CO_2$ hydrogenation to methanol over $Cu/CeO_2$ and $Cu/ZrO_2$ catalysts: tuning methanol selectivity via metal-support interaction. J Energy Chem 40:22–30
18. Wang WW, Qu ZP, Song LX et al (2020) An investigation of Zr/Ce ratio influencing the catalytic performance of $CuO/Ce_{1-x}Zr_xO_2$ catalyst for $CO_2$ hydrogenation to $CH_3OH$. J Energy Chem 47:18–28
19. Wang WW, Qu ZP, Song LX et al (2020) Probing into the multifunctional role of copper species and reaction pathway on copper-cerium-zirconium catalysts for $CO_2$ hydrogenation to methanol using high pressure in situ DRIFTS. J Catal 382:129–140
20. Wang JJ, Lu SM, Li J et al (2015) A remarkable difference in $CO_2$ hydrogenation to methanol on Pd nanoparticles supported inside and outside of carbon nanotubes. Chem Commun 51(99):17615–17618
21. Xu JH, Su X, Liu XY et al (2016) Methanol synthesis from $CO_2$ and $H_2$ over $Pd/ZnO/Al_2O_3$: catalyst structure dependence of methanol selectivity. Appl Catal A Gen 514:51–59
22. Wang JJ, Li GN, Li ZL et al (2017) A highly selective and stable $ZnO\text{-}ZrO_2$ solid solution catalyst for $CO_2$ hydrogenation to methanol. Sci Adv 3(10):e1701290
23. Han Z, Tang CZ, Sha F et al (2021) $CO_2$ hydrogenation to methanol on $ZnO\text{-}ZrO_2$ solid solution catalysts with ordered mesoporous structure. J Catal 396:242–250
24. Han Z, Tang CZ, Wang JJ et al (2021) Atomically dispersed $Pt^{n+}$ species as highly active sites in $Pt/In_2O_3$ catalysts for methanol synthesis from $CO_2$ hydrogenation. J Catal 394:236–244
25. Hu JT, Yu L, Deng J et al (2021) Sulfur vacancy-rich $MoS_2$ as a catalyst for the hydrogenation of $CO_2$ to methanol. Nat Catal 4(3):242–250
26. Wang JJ, Meeprasert J, Han Z et al (2022) Highly dispersed Cd cluster supported on $TiO_2$ as an efficient catalyst for $CO_2$ hydrogenation to methanol. Chin J Catal 43(3):761–770
27. Liu QG, Yang XF, Li L et al (2017) Direct catalytic hydrogenation of $CO_2$ to formate over a Schiff-base-mediated gold nanocatalyst. Nat Commun 8:1407
28. Shao XZ, Yang XF, Xu JM et al (2019) Iridium single-atom catalyst performing a quasi-homogeneous hydrogenation transformation of $CO_2$ to formate. Chem 5(3):693–705
29. Pan XL, Jiao F, Miao DY et al (2021) Oxide-zeolite-based composite catalyst concept that enables syngas chemistry beyond Fischer-Tropsch synthesis. Chem Rev 121(11):6588–6609
30. Su X, Xu JH, Liang BL et al (2016) Catalytic carbon dioxide hydrogenation to methane: a review of recent studies. J Energy Chem 25(4):553–565
31. Lin QQ, Liu XY, Jiang Y et al (2014) Crystal phase effects on the structure and performance of ruthenium nanoparticles for $CO_2$ hydrogenation. Catal Sci Technol 4(7):2058–2063
32. Xu JH, Su X, Duan HM et al (2016) Influence of pretreatment temperature on catalytic performance of rutile $TiO_2$-supported ruthenium catalyst in $CO_2$ methanation. J Catal 333:227–237
33. Gao LJ, Fu Q, Wei MM et al (2016) Enhanced nickel-catalyzed methanation confined under hexagonal boron nitride shells. ACS Catal 6(10):6814–6822
34. Pan QS, Peng JX, Sun TJ et al (2014) Insight into the reaction route of $CO_2$ methanation: promotion effect of medium basic sites. Catal Commun 45:74–78
35. Pan QS, Peng JX, Wang S et al (2014) In situ FTIR spectroscopic study of the $CO_2$ methanation mechanism on $Ni/Ce_{0.5}Zr_{0.5}O_2$. Catal Sci Technol 4(2):502–509
36. Gao J, Jiang Q, Liu YF et al (2018) Probing the enhanced catalytic activity of carbon nanotube supported $Ni\text{-}LaO_x$ hybrids for the $CO_2$ reduction reaction. Nanoscale 10(29):14207–14219
37. Li J, Lin YP, Pan XL et al (2019) Enhanced $CO_2$ methanation activity of Ni/anatase catalyst by tuning strong metal-support interactions. ACS Catal 9(7):6342–6348
38. Ye RP, Liao L, Reina TR et al (2021) Engineering $Ni/SiO_2$ catalysts for enhanced $CO_2$ methanation. Fuel 285:119151
39. Liao L, Chen LD, Ye RP et al (2021) Robust nickel silicate catalysts with high Ni loading for $CO_2$ methanation. Chem Asian J 16(6):678–689
40. Zhang YR, Zhang Z, Yang XF et al (2020) Tuning selectivity of $CO_2$ hydrogenation by modulating the strong metal–support interaction over $Ir/TiO_2$ catalysts. Green Chem 22(20):6855–6861

41. Zhang YR, Yan WJ, Qi HF et al (2022) Strong metal-support interaction of Ru on $TiO_2$ derived from the co-reduction mechanism of $Ru_xTi_{1-x}O_2$ interphase. ACS Catal 12(3):1697–1705
42. Xin H, Lin L, Li RT et al (2022) Overturning $CO_2$ hydrogenation selectivity with high activity via reaction-induced strong metal-support interactions. J Am Chem Soc 144(11):4874–4882
43. Chen XD, Su X, Su HY et al (2017) Theoretical insights and the corresponding construction of supported metal catalysts for highly selective $CO_2$ to CO conversion. ACS Catal 7(7):4613–4620
44. Li XY, Lin J, Li L et al (2020) Controlling $CO_2$ hydrogenation selectivity by metal-supported electron transfer. Angew Chem Int Ed 59(45):19983–19989
45. Zhang XB, Han SB, Zhu BE et al (2020) Reversible loss of core–shell structure for Ni–Au bimetallic nanoparticles during $CO_2$ hydrogenation. Nat Catal 3(4):411–417
46. Guo LS, Sun J, Ji XW et al (2018) Directly converting carbon dioxide to linear α-olefins on bio-promoted catalysts. Commun Chem 1:11
47. Liang BL, Duan HM, Sun T et al (2019) Effect of Na promoter on Fe-based catalyst for $CO_2$ hydrogenation to alkenes. ACS Sustain Chem Eng 7(1):925–932
48. Han Y, Fang CY, Ji XW et al (2020) Interfacing with carbonaceous potassium promoters boosts catalytic $CO_2$ hydrogenation of iron. ACS Catal 10(20):12098–12108
49. Yao RW, Wei J, Ge QJ et al (2021) Monometallic iron catalysts with synergistic Na and S for higher alcohols synthesis via $CO_2$ hydrogenation. Appl Catal B Environ 298:120556
50. Lohr TL, Marks TJ (2015) Orthogonal tandem catalysis. Nat Chem 7(6):477–482
51. Wei J, Sun J, Wen ZY et al (2016) New insights into the effect of sodium on $Fe_3O_4$-based nanocatalysts for $CO_2$ hydrogenation to light olefins. Catal Sci Technol 6(13):4786–4793
52. Liang BL, Sun T, Ma JG et al (2019) Mn decorated Na/Fe catalysts for $CO_2$ hydrogenation to light olefins. Catal Sci Technol 9(2):456–464
53. Jiao F, Li JJ, Pan XL et al (2016) Selective conversion of syngas to light olefins. Science 351(6277):1065–1068
54. Li J, Yu T, Miao DY et al (2019) Carbon dioxide hydrogenation to light olefins over ZnO-$Y_2O_3$ and SAPO-34 bifunctional catalysts. Catal Commun 129:105711
55. Li ZL, Wang JJ, Qu YZ et al (2017) Highly selective conversion of carbon dioxide to lower olefins. ACS Catal 7(12):8544–8548
56. Ni YM, Chen ZY, Fu Y et al (2018) Selective conversion of $CO_2$ and $H_2$ into aromatics. Nat Commun 9:3457
57. Li ZL, Qu YZ, Wang JJ et al (2019) Highly selective conversion of carbon dioxide to aromatics over tandem catalysts. Joule 3(2):570–583
58. Wei J, Yao RW, Ge QJ et al (2021) Precisely regulating Brønsted acid sites to promote the synthesis of light aromatics via $CO_2$ hydrogenation. Appl Catal B Environ 283:119648
59. Zhu PF, Sun J, Yang GH et al (2017) Tandem catalytic synthesis of benzene from $CO_2$ and $H_2$. Catal Sci Technol 7(13):2695–2699
60. Wei J, Ge QJ, Yao RW et al (2017) Directly converting $CO_2$ into a gasoline fuel. Nat Commun 8:15174
61. Wei J, Yao RW, Ge QJ et al (2018) Catalytic hydrogenation of $CO_2$ to isoparaffins over Fe-based multifunctional catalysts. ACS Catal 8(11):9958–9967
62. Noreen A, Li MQ, Fu YJ et al (2020) One-pass hydrogenation of $CO_2$ to multibranched isoparaffins over bifunctional zeolite-based catalysts. ACS Catal 10(23):14186–14194
63. Wei J, Yao RW, Han Y et al (2021) Towards the development of the emerging process of $CO_2$ heterogenous hydrogenation into high-value unsaturated heavy hydrocarbons. Chem Soc Rev 50(19):10764–10805
64. Ye X, Yang CY, Pan XL et al (2020) Highly selective hydrogenation of $CO_2$ to ethanol via designed bifunctional $Ir_1$-$In_2O_3$ single-atom catalyst. J Am Chem Soc 142(45):19001–19005
65. Ye X, Ma JG, Yu WG et al (2022) Construction of bifunctional single-atom catalysts on the optimized β-$Mo_2C$ surface for highly selective hydrogenation of $CO_2$ into ethanol. J Energy Chem 67:184–192
66. Yao SD, Gu LJ, Sun CY et al (2009) Combined methane $CO_2$ reforming and dehydroaromatization for enhancing the catalyst stability. Ind Eng Chem Res 48(2):713–718
67. Zhang JC, Ge BH, Liu TF et al (2020) Robust ruthenium-saving catalyst for high-temperature carbon dioxide reforming of methane. ACS Catal 10(1):783–791
68. Dong JH, Fu Q, Li HB et al (2020) Reaction-induced strong metal-support interactions between metals and inert boron nitride nanosheets. J Am Chem Soc 142(40):17167–17174
69. Wang YH, Zhang ZX, Lei LJ et al (2021) Defect-dependent selective C-H/C–C bond cleavage of propane in the presence of $CO_2$ over FeNi/ceria catalysts. ACS Sustain Chem Eng 9(51):17301–17309
70. Wang JP, Liu M, Li JJ et al (2022) Elucidating the active-phase evolution of Fe-based catalysts during isobutane dehydrogenation with and without $CO_2$ in feed gas. ACS Catal 12(10):5930–5938
71. Jeong MH, Lee DH, Moon JW et al (2022) Oxidative dehydrogenation of ethane and subsequent $CO_2$ activation on Ce-incorporated $FeTiO_x$ metal oxides. Chem Eng J 433:134621
72. Jiang QQ, Chen ZP, Tong JH et al (2017) Direct thermolysis of $CO_2$ into CO and $O_2$. Chem Commun 53(6):1188–1191
73. Jiang QQ, Chen ZP, Tong JH et al (2016) Catalytic function of $IrO_x$ in the two-step thermochemical $CO_2$-splitting reaction at high temperatures. ACS Catal 6(2):1172–1180
74. Li H, Goldbach A, Li WZ et al (2008) $CO_2$ decomposition over Pd membrane surfaces. J Phys Chem B 112(39):12182–12184
75. Zhao GD, Zhang Y, Zhang HY et al (2015) Direct synthesis of propylene carbonate from propylene and carbon dioxide catalyzed by quaternary ammonium heteropolyphosphatotungstate-TBAB system. J Energy Chem 24(3):353–358
76. Chen YD, Wang H, Qin ZX et al (2019) $Ti_xCe_{1-x}O_2$ nanocomposites: a monolithic catalyst for the direct conversion of carbon dioxide and methanol to dimethyl carbonate. Green Chem 21(17):4642–4649
77. Wang WL, Wang YQ, Li CY et al (2017) State-of-the-art multifunctional heterogeneous POP catalyst for cooperative transformation of $CO_2$ to cyclic carbonates. ACS Sustain Chem Eng 5(6):4523–4528
78. Jayakumar S, Li H, Tao L et al (2018) Cationic Zn-porphyrin immobilized in mesoporous silicas as bifunctional catalyst for $CO_2$ cycloaddition reaction under cocatalyst free conditions. ACS Sustain Chem Eng 6:9237–9245
79. Chen J, Zhong MM, Tao L et al (2018) The cooperation of porphyrin-based porous polymer and thermal-responsive ionic liquid for efficient $CO_2$ cycloaddition reaction. Green Chem 20(4):903–911
80. Liu L, Jayakumar S, Chen J et al (2021) Synthesis of bifunctional porphyrin polymers for catalytic conversion of dilute $CO_2$ to cyclic carbonates. ACS Appl Mater Interfaces 13(25):29522–29531
81. Wu ZL, Sun L, Liu QG et al (2017) A Schiff base-modified silver catalyst for efficient fixation of $CO_2$ as carboxylic acid at ambient pressure. Green Chem 19(9):2080–2085
82. Wu ZL, Liu QG, Yang XF et al (2017) Knitting aryl network polymers-incorporated Ag nanoparticles: a mild and efficient catalyst for the fixation of $CO_2$ as carboxylic acid. ACS Sustain Chem Eng 5(11):9634–9639

83. Wang GQ, Jiang M, Ji GJ et al (2020) Bifunctional heterogeneous Ru/POP catalyst embedded with alkali for the N-formylation of amine and $CO_2$. ACS Sustain Chem Eng 8(14):5576–5583
84. Chen C, Zhu XR, Wen XJ et al (2020) Coupling $N_2$ and $CO_2$ in $H_2O$ to synthesize urea under ambient conditions. Nat Chem 12(8):717–724
85. de Luna P, Hahn C, Higgins D et al (2019) What would it take for renewably powered electrosynthesis to displace petrochemical processes? Science 364(6438):eaav3506
86. Song YF, Zhang XM, Xie K et al (2019) High-temperature $CO_2$ electrolysis in solid oxide electrolysis cells: developments, challenges, and prospects. Adv Mater 31(50):e1902033
87. Zhan ZL, Zhao L (2010) Electrochemical reduction of $CO_2$ in solid oxide electrolysis cells. J Power Sources 195(21):7250–7254
88. Zhang XM, Song YF, Wang GX et al (2017) Co-electrolysis of $CO_2$ and $H_2O$ in high-temperature solid oxide electrolysis cells: recent advance in cathodes. J Energy Chem 26(5):839–853
89. Xie K, Zhang YQ, Meng GY et al (2011) Direct synthesis of methane from $CO_2/H_2O$ in an oxygen-ion conducting solid oxide electrolyser. Energy Environ Sci 4(6):2218
90. Yan JB, Chen H, Dogdibegovic E et al (2014) High-efficiency intermediate temperature solid oxide electrolyzer cells for the conversion of carbon dioxide to fuels. J Power Sources 252:79–84
91. Song YF, Zhou ZW, Zhang XM et al (2018) Pure $CO_2$ electrolysis over an Ni/YSZ cathode in a solid oxide electrolysis cell. J Mater Chem A 6(28):13661–13667
92. Zhou YJ, Zhou ZW, Song YF et al (2018) Enhancing $CO_2$ electrolysis performance with vanadium-doped perovskite cathode in solid oxide electrolysis cell. Nano Energy 50:43–51
93. Hu SQ, Zhang LX, Liu HY et al (2019) Detrimental phase evolution triggered by Ni in perovskite-type cathodes for $CO_2$ electroreduction. J Energy Chem 36:87–94
94. Hu SQ, Zhang LX, Liu HY et al (2019) Alkaline-earth elements (Ca, Sr and Ba) doped $LaFeO_{3-\delta}$ cathodes for $CO_2$ electroreduction. J Power Sources 443:227268
95. Hu SQ, Zhang LX, Cai LL et al (2020) Iron stabilized 1/3 A-site deficient La–Ti–O perovskite cathodes for efficient $CO_2$ electroreduction. J Mater Chem A 8(40):21053–21061
96. Liu QX, Song YF, Li RT et al (2021) A vanadium-doped BSCF perovskite for $CO_2$ electrolysis in solid oxide electrolysis cells. Int J Hydrog Energy 46(38):19814–19821
97. Zhou YJ, Lin L, Song YF et al (2020) Pd single site-anchored perovskite cathode for $CO_2$ electrolysis in solid oxide electrolysis cells. Nano Energy 71:104598
98. Zhang XM, Song YF, Guan F et al (2018) Enhancing electrocatalytic $CO_2$ reduction in solid oxide electrolysis cell with $Ce_{0.9}Mn_{0.1}O_{2-\delta}$ nanoparticles-modified LSCM-GDC cathode. J Catal 359:8–16
99. Lv HF, Zhou YJ, Zhang XM et al (2019) Infiltration of $Ce_{0.8}Gd_{0.2}O_{1.9}$ nanoparticles on $Sr_2Fe_{1.5}Mo_{0.5}O_{6-\delta}$ cathode for $CO_2$ electroreduction in solid oxide electrolysis cell. J Energy Chem 35:71–78
100. Feng WC, Song YF, Zhang XM et al (2020) Platinum-decorated ceria enhances $CO_2$ electroreduction in solid oxide electrolysis cells. ChemSusChem 13(23):6290–6295
101. Lv HF, Lin L, Zhang XM et al (2019) In situ exsolved $FeNi_3$ nanoparticles on nickel doped $Sr_2Fe_{1.5}Mo_{0.5}O_{6-\delta}$ perovskite for efficient electrochemical $CO_2$ reduction reaction. J Mater Chem A 7(19):11967–11975
102. Lv HF, Lin L, Zhang XM et al (2020) In situ investigation of reversible exsolution/dissolution of CoFe alloy nanoparticles in a co-doped $Sr_2Fe_{1.5}Mo_{0.5}O_{6-\delta}$ cathode for $CO_2$ electrolysis. Adv Mater 32(6):e1906193
103. Lv HF, Liu TF, Zhang XM et al (2020) Atomic-scale insight into exsolution of CoFe alloy nanoparticles in $La_{0.4}Sr_{0.6}Co_{0.2}Fe_{0.7}Mo_{0.1}O_{3-\delta}$ with efficient $CO_2$ electrolysis. Angew Chem Int Ed 59(37):15968–15973
104. Lv HF, Lin L, Zhang XM et al (2021) Promoting exsolution of RuFe alloy nanoparticles on $Sr_2Fe_{1.4}Ru_{0.1}Mo_{0.5}O_{6-\delta}$ via repeated redox manipulations for $CO_2$ electrolysis. Nat Commun 12:5665
105. Zhang LX, Li XB, Lu JM et al (2021) In situ dispersed nano-Au on Zr-suboxides as active cathode for direct $CO_2$ electroreduction in solid oxide electrolysis cells. Nano Lett 21(16):6952–6959
106. Hori Y, Kikuchi K, Suzuki S (1985) Production of CO and $CH_4$ in electrochemical reduction of $CO_2$ at metal electrodes in aqueous hydrogencarbonate solution. Chem Lett 14(11):1695–1698
107. Hori Y, Kikuchi K, Murata A et al (1986) Production of methane and ethylene in electrochemical reduction of carbon dioxide at copper electrode in aqueous hydrogencarbonate solution. Chem Lett 15(6):897–898
108. Jiang XL, Cai F, Gao DF et al (2016) Electrocatalytic reduction of carbon dioxide over reduced nanoporous zinc oxide. Electrochem Commun 68:67–70
109. Gao DF, Cai F, Wang GX et al (2017) Nanostructured heterogeneous catalysts for electrochemical reduction of $CO_2$. Curr Opin Green Sustain Chem 3:39–44
110. Yan CC, Lin L, Gao DF et al (2018) Selective $CO_2$ electroreduction over an oxide-derived gallium catalyst. J Mater Chem A 6(40):19743–19749
111. Gao DF, Yan CC, Wang GX et al (2018) Pd/C catalysts for $CO_2$ electroreduction to CO: Pd loading effect. J Electrochem 24(6):757–765
112. Yu Q, Guo CX, Ge JY et al (2020) Morphology controlling of silver by plasma engineering for electrocatalytic carbon dioxide reduction. J Power Sources 453:227846
113. Lin XZ, Ma WG, Sun KJ et al (2021) $[AuAg_{26}(SR)_{18}S]^-$: open shell structure and high faradaic efficiency in electrochemical reduction of $CO_2$ to CO. J Phys Chem Lett 12(1):552–557
114. Ye K, Liu TF, Song YP et al (2021) Tailoring the interactions of heterogeneous $Ag_2S$/Ag interface for efficient $CO_2$ electroreduction. Appl Catal B Environ 296:120342
115. Gao DF, Li HF, Wei PF et al (2022) Electrochemical synthesis of catalytic materials for energy catalysis. Chin J Catal 43(4):1001–1016
116. Gao DF, Liu TF, Wang GX et al (2021) Structure sensitivity in single-atom catalysis toward $CO_2$ electroreduction. ACS Energy Lett 6(2):713–727
117. Zang YP, Wei PF, Li HF et al (2022) Catalyst design for electrolytic $CO_2$ reduction toward low-carbon fuels and chemicals. Electrochem Energy Rev. https://doi.org/10.1007/s41918-022-00140-y
118. Gao DF, Zhou H, Cai F et al (2017) Switchable $CO_2$ electroreduction via engineering active phases of Pd nanoparticles. Nano Res 10(6):2181–2191
119. Gao DF, Zhou H, Cai F et al (2018) Pd-containing nanostructures for electrochemical $CO_2$ reduction reaction. ACS Catal 8(2):1510–1519
120. Yin Z, Gao DF, Yao SY et al (2016) Highly selective palladium-copper bimetallic electrocatalysts for the electrochemical reduction of $CO_2$ to CO. Nano Energy 27:35–43
121. Cai F, Gao DF, Si R et al (2017) Effect of metal deposition sequence in carbon-supported Pd-Pt catalysts on activity towards $CO_2$ electroreduction to formate. Electrochem Commun 76:1–5
122. Cai F, Gao DF, Zhou H et al (2017) Electrochemical promotion of catalysis over Pd nanoparticles for $CO_2$ reduction. Chem Sci 8(4):2569–2573
123. Gao DF, Zhang Y, Zhou ZW et al (2017) Enhancing $CO_2$ electroreduction with the metal-oxide interface. J Am Chem Soc 139(16):5652–5655

124. Yan CC, Li HB, Ye YF et al (2018) Coordinatively unsaturated nickel–nitrogen sites towards selective and high-rate $CO_2$ electroreduction. Energy Environ Sci 11(5):1204–1210
125. Yang HB, Hung SF, Liu S et al (2018) Atomically dispersed Ni(i) as the active site for electrochemical $CO_2$ reduction. Nat Energy 3(2):140–147
126. Lin L, Li HB, Yan CC et al (2019) Synergistic catalysis over iron-nitrogen sites anchored with cobalt phthalocyanine for efficient $CO_2$ electroreduction. Adv Mater 31(41):e1903470
127. Zhang Z, Ma C, Tu YC et al (2019) Multiscale carbon foam confining single iron atoms for efficient electrocatalytic $CO_2$ reduction to CO. Nano Res 12(9):2313–2317
128. Ma SS, Su PP, Huang WJ et al (2019) Atomic Ni species anchored N-doped carbon hollow spheres as nanoreactors for efficient electrochemical $CO_2$ reduction. ChemCatChem 11(24):6092–6098
129. Liu S, Yang HB, Hung SF et al (2020) Elucidating the electrocatalytic $CO_2$ reduction reaction over a model single-atom nickel catalyst. Angew Chem Int Ed 59(2):798–803
130. Ding CM, Feng CC, Mei YH et al (2020) Carbon nitride embedded with transition metals for selective electrocatalytic $CO_2$ reduction. Appl Catal B Environ 268:118391
131. Ren XY, Liu S, Li HC et al (2020) Electron-withdrawing functional ligand promotes $CO_2$ reduction catalysis in single atom catalyst. Sci China Chem 63(12):1727–1733
132. Yao PF, Li TY, Qiu YL et al (2021) N-doped hierarchical porous carbon derived from bismuth salts decorated ZIF8 as a highly efficient electrocatalyst for $CO_2$ reduction. J Mater Chem A 9(1):320–326
133. Liu S, Yang HB, Su X et al (2019) Rational design of carbon-based metal-free catalysts for electrochemical carbon dioxide reduction: a review. J Energy Chem 36:95–105
134. Yao PF, Qiu YL, Zhang TT et al (2019) N-doped nanoporous carbon from biomass as a highly efficient electrocatalyst for the $CO_2$ reduction reaction. ACS Sustain Chem Eng 7(5):5249–5255
135. Cheng CF, Shao JQ, Wei PF et al (2021) Nitrogen and boron co-doped carbon spheres for carbon dioxide electroreduction. ChemNanoMat 7(6):635–640
136. Gao DF, Wang J, Wu HH et al (2015) pH effect on electrocatalytic reduction of $CO_2$ over Pd and Pt nanoparticles. Electrochem Commun 55:1–5
137. Jiang XL, Li HF, Yang YY et al (2020) pH dependence of $CO_2$ electroreduction selectivity over size-selected Au nanoparticles. J Mater Sci 55(28):13916–13926
138. Lin L, Li HB, Wang Y et al (2021) Temperature-dependent $CO_2$ electroreduction over Fe-N-C and Ni-N-C single-atom catalysts. Angew Chem Int Ed 60(51):26582–26586
139. Zhong HX, Qiu YL, Zhang TT et al (2016) Bismuth nanodendrites as a high performance electrocatalyst for selective conversion of $CO_2$ to formate. J Mater Chem A 4(36):13746–13753
140. Su PP, Xu WB, Qiu YL et al (2018) Ultrathin bismuth nanosheets as a highly efficient $CO_2$ reduction electrocatalyst. ChemSusChem 11(5):848–853
141. Zhang TT, Qiu YL, Yao PF et al (2019) Bi-modified Zn catalyst for efficient $CO_2$ electrochemical reduction to formate. ACS Sustain Chem Eng 7(18):15190–15196
142. Shi YM, Ji Y, Long J et al (2020) Unveiling hydrocerussite as an electrochemically stable active phase for efficient carbon dioxide electroreduction to formate. Nat Commun 11:3415
143. Li ZJ, Cao A, Zheng Q et al (2021) Elucidation of the synergistic effect of dopants and vacancies on promoted selectivity for $CO_2$ electroreduction to formate. Adv Mater 33(2):e2005113
144. Ye K, Zhou ZW, Shao JQ et al (2020) In situ reconstruction of a hierarchical Sn-Cu/$SnO_x$ core/shell catalyst for high-performance $CO_2$ electroreduction. Angew Chem Int Ed 59(12):4814–4821
145. Ye K, Cao A, Shao JQ et al (2020) Synergy effects on Sn-Cu alloy catalyst for efficient $CO_2$ electroreduction to formate with high mass activity. Sci Bull 65(9):711–719
146. Shao JQ, Wang Y, Gao DF et al (2020) Copper-indium bimetallic catalysts for the selective electrochemical reduction of carbon dioxide. Chin J Catal 41(9):1393–1400
147. Zheng TT, Liu CX, Guo CX et al (2021) Copper-catalysed exclusive $CO_2$ to pure formic acid conversion via single-atom alloying. Nat Nanotechnol 16(12):1386–1393
148. Qiu YL, Zhong HX, Zhang TT et al (2017) Copper electrode fabricated via pulse electrodeposition: toward high methane selectivity and activity for $CO_2$ electroreduction. ACS Catal 7(9):6302–6310
149. Lin L, Liu TF, Xiao JP et al (2020) Enhancing $CO_2$ electroreduction to methane with a cobalt phthalocyanine and zinc-nitrogen-carbon tandem catalyst. Angew Chem Int Ed 59(50):22408–22413
150. Chen RX, Su HY, Liu DY et al (2020) Highly selective production of ethylene by the electroreduction of carbon monoxide. Angew Chem Int Ed 59(1):154–160
151. Ma WC, Xie SJ, Liu TT et al (2020) Electrocatalytic reduction of $CO_2$ to ethylene and ethanol through hydrogen-assisted C–C coupling over fluorine-modified copper. Nat Catal 3(6):478–487
152. Ji YL, Chen Z, Wei RL et al (2022) Selective CO-to-acetate electroreduction via intermediate adsorption tuning on ordered Cu–Pd sites. Nat Catal 5(4):251–258
153. Gao DF, Arán-Ais RM, Jeon HS et al (2019) Rational catalyst and electrolyte design for $CO_2$ electroreduction towards multicarbon products. Nat Catal 2(3):198–210
154. Arán-Ais RM, Scholten F, Kunze S et al (2020) The role of in situ generated morphological motifs and Cu(i) species in $C_{2+}$ product selectivity during $CO_2$ pulsed electroreduction. Nat Energy 5(4):317–325
155. Sang JQ, Wei PF, Liu TF et al (2022) A reconstructed $Cu_2P_2O_7$ catalyst for selective $CO_2$ electroreduction to multicarbon products. Angew Chem Int Ed 61(5):e202114238
156. Li HF, Wei PF, Gao DF et al (2022) In situ Raman spectroscopy studies for electrochemical $CO_2$ reduction over Cu catalysts. Curr Opin Green Sustain Chem 34:100589
157. Velasco-Vélez JJ, Chuang CH, Gao DF et al (2020) On the activity/selectivity and phase stability of thermally grown copper oxides during the electrocatalytic reduction of $CO_2$. ACS Catal 10(19):11510–11518
158. Xiao H, Goddard WA 3rd, Cheng T et al (2017) Cu metal embedded in oxidized matrix catalyst to promote $CO_2$ activation and CO dimerization for electrochemical reduction of $CO_2$. Proc Natl Acad Sci USA 114(26):6685–6688
159. Timoshenko J, Bergmann A, Rettenmaier C et al (2022) Steering the structure and selectivity of $CO_2$ electroreduction catalysts by potential pulses. Nat Catal 5(4):259–267
160. Gao DF (2022) Revealing structure-selectivity correlations in pulsed $CO_2$ electrolysis via time-resolved operando synchrotron X-ray studies. Nano Res. 15(8):6860–6861
161. Li HF, Liu TF, Wei PF et al (2021) High-rate $CO_2$ electroreduction to $C_{2+}$ products over a copper-copper iodide catalyst. Angew Chem Int Ed 60(26):14329–14333
162. Zhu YT, Cui XY, Liu HL et al (2021) Tandem catalysis in electrochemical $CO_2$ reduction reaction. Nano Res 14(12):4471–4486
163. Huang JF, Mensi M, Oveisi E et al (2019) Structural sensitivities in bimetallic catalysts for electrochemical $CO_2$ reduction revealed by Ag-Cu nanodimers. J Am Chem Soc 141(6):2490–2499
164. Wang XL, de Araújo JF, Ju W et al (2019) Mechanistic reaction pathways of enhanced ethylene yields during electroreduction of $CO_2$-CO co-feeds on Cu and Cu-tandem electrocatalysts. Nat Nanotechnol 14(11):1063–1070

165. Xu D, Yang HQ, Hong XL et al (2021) Tandem catalysis of direct $CO_2$ hydrogenation to higher alcohols. ACS Catal 11(15):8978–8984
166. Liu XL, Wang MH, Yin HR et al (2020) Tandem catalysis for hydrogenation of CO and $CO_2$ to lower olefins with bifunctional catalysts composed of spinel oxide and SAPO-34. ACS Catal 10(15):8303–8314
167. Ma ZQ, Porosoff MD (2019) Development of tandem catalysts for $CO_2$ hydrogenation to olefins. ACS Catal 9(3):2639–2656
168. Gao DF, Cai F, Xu QQ et al (2014) Gas-phase electrocatalytic reduction of carbon dioxide using electrolytic cell based on phosphoric acid-doped polybenzimidazole membrane. J Energy Chem 23(6):694–700
169. Gao DF, Wei PF, Li HF et al (2021) Designing electrolyzers for electrocatalytic $CO_2$ reduction. Acta Phys-Chim Sin 37(5):2009021
170. Yin ZL, Peng HQ, Wei X et al (2019) An alkaline polymer electrolyte $CO_2$ electrolyzer operated with pure water. Energy Environ Sci 12(8):2455–2462
171. Wei PF, Li HF, Lin L et al (2020) $CO_2$ electrolysis at industrial current densities using anion exchange membrane based electrolyzers. Sci China Chem 63(12):1711–1715
172. Wakerley D, Lamaison S, Wicks J et al (2022) Gas diffusion electrodes, reactor designs and key metrics of low-temperature $CO_2$ electrolysers. Nat Energy 7(2):130–143
173. Endrődi B, Kecsenovity E, Samu A et al (2019) Multilayer electrolyzer stack converts carbon dioxide to gas products at high pressure with high efficiency. ACS Energy Lett 4(7):1770–1777
174. Rabinowitz JA, Kanan MW (2020) The future of low-temperature carbon dioxide electrolysis depends on solving one basic problem. Nat Commun 11:5231
175. Ozden A, García de Arquer FP, Huang JE et al (2022) Carbon-efficient carbon dioxide electrolysers. Nat Sustain 5(7):563–573
176. Larrazábal GO, Strøm-Hansen P, Heli JP et al (2019) Analysis of mass flows and membrane cross-over in $CO_2$ reduction at high current densities in an MEA-type electrolyzer. ACS Appl Mater Interfaces 11(44):41281–41288
177. Ma M, Clark EL, Therkildsen KT et al (2020) Insights into the carbon balance for $CO_2$ electroreduction on Cu using gas diffusion electrode reactor designs. Energy Environ Sci 13(3):977–985
178. Siritanaratkul B, Forster M, Greenwell F et al (2022) Zero-gap bipolar membrane electrolyzer for carbon dioxide reduction using acid-tolerant molecular electrocatalysts. J Am Chem Soc 144(17):7551–7556
179. Kim JY, Zhu P, Chen FY et al (2022) Recovering carbon losses in $CO_2$ electrolysis using a solid electrolyte reactor. Nat Catal 5(4):288–299
180. Fujinuma N, Ikoma A, Lofland SE (2020) Highly efficient electrochemical $CO_2$ reduction reaction to CO with one-pot synthesized co-pyridine-derived catalyst incorporated in a nafion-based membrane electrode assembly. Adv Energy Mater 10(39):2001645
181. Huang JE, Li FW, Ozden A et al (2021) $CO_2$ electrolysis to multicarbon products in strong acid. Science 372(6546):1074–1078
182. Monteiro MCO, Dattila F, Hagedoorn B et al (2021) Absence of $CO_2$ electroreduction on copper, gold and silver electrodes without metal cations in solution. Nat Catal 4(8):654–662
183. Monteiro MCO, Philips MF, Schouten KJP et al (2021) Efficiency and selectivity of $CO_2$ reduction to CO on gold gas diffusion electrodes in acidic media. Nat Commun 12:4943
184. Gu J, Liu S, Ni WY et al (2022) Modulating electric field distribution by alkali cations for $CO_2$ electroreduction in strongly acidic medium. Nat Catal 5(4):268–276
185. Ozden A, Wang YH, Li FW et al (2021) Cascade $CO_2$ electroreduction enables efficient carbonate-free production of ethylene. Joule 5(3):706–719
186. Wang Y, Zhang ZZ, Zhang LN et al (2018) Visible-light driven overall conversion of $CO_2$ and $H_2O$ to $CH_4$ and $O_2$ on 3D-SiC@2D-$MoS_2$ heterostructure. J Am Chem Soc 140(44):14595–14598
187. Hou TT, Luo NC, Cui YT et al (2019) Selective reduction of $CO_2$ to CO under visible light by controlling coordination structures of $CeO_x$-S/$ZnIn_2S_4$ hybrid catalysts. Appl Catal B Environ 245:262–270
188. Gao W, Bai XW, Gao YY et al (2020) Anchoring of black phosphorus quantum dots onto $WO_3$ nanowires to boost photocatalytic $CO_2$ conversion into solar fuels. Chem Commun 56(56):7777–7780
189. Wang Y, Shang XT, Shen JN et al (2020) Direct and indirect Z-scheme heterostructure-coupled photosystem enabling cooperation of $CO_2$ reduction and $H_2O$ oxidation. Nat Commun 11:3043
190. Li RG, Cheng WH, Richter MH et al (2021) Unassisted highly selective gas-phase $CO_2$ reduction with a plasmonic Au/p-GaN photocatalyst using $H_2O$ as an electron donor. ACS Energy Lett 6(5):1849–1856
191. Zhang HF, Chen Y, Wang H et al (2020) Carbon encapsulation of organic-inorganic hybrid perovskite toward efficient and stable photo-electrochemical carbon dioxide reduction. Adv Energy Mater 10(44):2002105


**Guoxiong Wang** received his B.S. from Wuhan University in 2000 and PhD in physical chemistry from DICP in 2006. After working at Catalysis Research Center, Hokkaido University, Japan (2007–2010) as a postdoctoral researcher, he joined State Key Laboratory of Catalysis, DICP as an associate professor and was promoted as full professor in 2015. His research interests include highly efficient catalytic materials and processes for electrochemical energy conversion and storage.

**Rui Cai** received his B.S. from Nanjing University in 1999 and PhD in physical chemistry from DICP in 2005. After postdoctoral studies in the University of California, Riverside (2006–2010), he joined DICP in 2010. He is currently a full professor and deputy director of DICP and Qingdao Institute of Bioenergy and Bioprocess Technology. His main research interests include separation and catalysis of inorganic membrane materials as well as strategic research of energy science and technology.